Pergamon

Geochimica et Cosmochimica Acta, Vol. 67, No. 18, pp. 3499–3518, 2003

0016-7037/03 $30.00 + .00

doi:10.1016/S0016-7037(03)00134-0

Petrogenesis of lunar meteorite EET 96008

MAHESH ANAND,[1,*] LAWRENCE A. TAYLOR,[1] CLIVE R. NEAL,[2] GREGORY A. SNYDER,[1] ALLAN PATCHEN,[1] YUJI SANO,[3] and KENTARO TERADA[4]

[1]Planetary Geosciences Institute, Department of Geological Sciences, University of Tennessee, Knoxville, TN 37996, USA
[2]Department of Civil Engineering & Geological Sciences, University of Notre Dame, Notre Dame, IN 46556, USA
[3]Center for Environmental Research, Ocean Research Institute, The University of Tokyo, Nakanoku, Tokyo, 164-8639, Japan
[4]Department of Earth & Planetary Sciences, Hiroshima University, Higashi-Hiroshima, 739-8526, Japan

(*Received August* 28, 2002; *accepted in revised form February* 14, 2003)

Abstract—Lunar meteorite EET 96008 is a fragmental breccia that predominantly consists of basaltic mineral clasts (0.5–2 mm), along with minor lithic fragments and breccia clasts. The matrix consists mainly of smaller mineral fragments (<0.5 mm), bound by glassy cement, the majority of which are pyroxene and plagioclase. The pyroxene possesses extensive exsolution lamellae. These lamellae, up to 1 μm in width, are atypical for mare-basalts. One of the distinguishing textures of EET 96008 is the presence of small pockets ($\sim$400 $\times$ 500 μm) of mesostasis areas consisting of coarse ($\sim$20 μm) intergrowths of ferroaugite, fayalite and Si-rich glass. Laths of ilmenite, armalcolite, apatite and whitlockite are also distributed in these areas. Ilmenite grains are abundant and dispersed throughout the thin sections. Chromite and ulvöspinel are present but in minor abundance. Troilite, generally rare in this rock, occurs as several grains in one pyroxene crystal. FeNi metal is conspicuously absent from this meteorite.

The molar Fe/Mn ratio in olivines and pyroxenes and the age of the meteorite are evidence for a lunar origin. The mineralogy of EET 96008 shows close affinity to a mare-basalt source, albeit with possible minor highland/non-mare components. The bulk-rock, major-, trace- and rare-earth-element (REE) contents are similar to that of very low-titanium (VLT) basalts, which have experienced extreme fractional crystallization to the point of silicate liquid immiscibility. Mineralogical and textural features of this sample suggest that at least some of the breccia components were derived from a slow-cooled magma. The mineralogy and petrology of EET 96008 is strikingly similar to the lunar meteorite EET 87521, and we support the conclusion that EET 96008 and EET 87521 should be paired.

Isochron ages of 3530 $\pm$ 270 Ma for apatite and 3519 $\pm$ 100 Ma for whitlockite of this rock are consistent with derivation from a mare-basalt precursor. These ages are within error of the low-Ti basalts, dated from the Apollo 12 and 15 sites. The whole-rock, platinum-group-element (PGE) contents of EET 96008 overlap with pristine low-Ti mare basalts, suggesting the presence of only a minimal extraterrestrial component. *Copyright © 2003 Elsevier Ltd*

1. INTRODUCTION

The six Apollo and three LUNA Missions provided the world with returned lunar rocks and soils that have formed the basis for our understanding of the origin and evolution of the Moon. There have been no follow-on, return-sample missions to the Moon in the years subsequent to 1976 (Luna 24). However, the discovery of meteorites that were blasted off the Moon by large bolide impacts has provided the science community with a different type of "returned" lunar samples. Indeed, these precious meteorites are likely to have originated from disparate locations on the Moon and have opened up an entirely new source of materials with which to further explore our only natural satellite.

During the 1995–1996 ANSMET field season, a 52.97-g lunar meteorite, the 16th, was collected from the Meteorite City icefield in the vicinity of Elephant Moraine and designated as EET 96008. It is only the second lunar breccia which consists dominantly of basaltic clasts. The rest of the lunar breccias in Apollo and lunar meteorite collections are predominantly made up of highlands-derived material. Based on mineralogy and petrology, Mikouchi (1999) classified EET 96008 as a fragmental breccia containing both mare and highland materials, but with a dominance of mare components. Warren and Ulff-Møller (1999) measured the bulk-chemical composition and suggested that EET 96008 consists of nearly pure Ti-poor mare-basalt (VLT); however, portions of the meteorite are rich in diverse clasts, including a highland impact-melt breccia. We were allocated two polished thin-sections (EET 96008,38 and EET 96008,39) and three 151- to 172-mg whole-rock splits of this meteorite.

* Author to whom correspondence should be addressed (anandm@utk.edu).

2. ANALYTICAL METHODS

Mineral and whole-rock (both major- and trace-element) chemical analyses were conducted on EET 96008. Mineral chemistry was determined on the two thin sections using a CAMECA SX-50 electron microprobe (EMP), at the University of Tennessee, operated at 15 kV and 20 nA, with 20-s count times for the majority of the elements. The mineral data were corrected using the Cameca PAP correction procedure. Each of the three whole-rock splits ($\sim$50 mg) was analyzed for trace elements by inductively coupled plasma mass spectrometry (ICP-MS) at the University of Notre Dame. All samples were processed in a class-1000 clean laboratory, and ultrapure reagents were used at all times. Full details of the methods used are given by Snyder et al. (1997), and Neal (2001). Representative portions of these three splits were combined and a 10-mg fraction was fused into a glass bead on a Mo-strip heater, in a nitrogen atmosphere. This glass was analyzed by

electron microprobe for major elements. Another portion was dissolved, passed through cation exchange columns, and analyzed by ICP-MS for the PGEs following the method of Ely et al. (1999), with data reduction and error analysis as detailed in Ely and Neal (2002). U-Pb age data, as well as REE contents, of phosphate grains in EET 96008 were obtained with an ion-microprobe (SHRIMP) at Hiroshima University, Japan, using the method described in Sano et al. (1999).

3. PETROGRAPHY

We have studied two thin sections of the lunar meteorite EET 96008 with a total area of 7.5 cm^2. EET 96008 is a fragmental polymict breccia mainly composed of individual mineral fragments (pyroxene and plagioclase, with minor olivine) and minor amounts of lithic and breccia clasts. The matrix is made up of fine-grained mafic minerals bound by dark glassy cement. The majority of the clasts in our samples consist dominantly of mare materials. However, there are a few clasts that resemble materials from lunar highlands or non-mare source regions. Our samples are also conspicuous in having a predominance of mesostasis areas that consist of intergrowths of coarse-grained ferroaugite (close to hedenbergite in composition) and fayalite with interstitial Si-rich glass. In the following subsections, petrography of thin sections examined is described in more detail followed by detailed account of the mineral chemistry observed in this rock. The representative mineral analyses from different clasts are presented in Table 1.

The thin sections contain evidence of several generations of brecciation, such as phenocrysts and clasts being contained within larger breccia clasts, which in turn are crosscut by later glass veins. The majority of the rock consists of single clasts of pyroxenes (up to 2 mm long) and plagioclases, set in a finer-grained matrix (Fig. 1a), which is a mixture of smaller (<0.5 mm) pyroxene and plagioclase fragments. The majority of pyroxene grains show exsolution lamellae, atypical of mare-basalts, and are pleochroic in plane-polarized light (PPL), indicating their Fe-rich nature.

Clast A is a euhedral olivine grain (~1 mm in size) containing a glass inclusion near the center (Fig. 1b). This grain shows pleochroism from pink to green in color, typical of fayalite, consistent with its Fe-rich composition (see section on mineral data). Whitlockite (10–50 μm) occurs along the contact of the glass with the fayalite host. An ilmenite grain is also present near the center of the olivine host.

Clast B is an unusual component of the breccia. It consists of a large plagioclase fragment (2–3 mm in size) enclosing laths of silica and small (~100 μm) grains of hedenbergite (Fig. 1c). A few Cr-spinel crystals also occur in the clast, associated with hedenbergite grains. The silica mass is probably tridymite, as evident from its crackled texture.

Clast C is a breccia clast, 1 mm in length, consisting of fine-grained plagioclase, olivine, and pyroxene grains in an impact-melt matrix (Fig. 1d). Because of the small grain size, it is difficult to establish the pyroxene type under transmitted light but EMP data (see section on mineral data) confirm that some Mg-rich orthopyroxene occur in this clast along with fairly Mg-rich olivine, and thus this clast has been termed as "Norite," indicating affinity to highland rocks.

An area ~2 × 2 mm across (Clast D) in our sample possesses a vesicular texture, similar to some of the lunar-regolith breccias (Fig. 1e). The white dashed line follows the outline of the regolith-looking clast. Medium-grained (100–200 μm) pyroxene and olivine grains are also present in this clast. However, native iron and glass spherules were not seen, and hence, it is not possible to ascribe a regolith origin to this clast.

Clast E is an impact-melt breccia of lunar-highlands derivation. The back-scatter electron image (BSE) of this area highlights the poorly crystallized nature of the impact melt and indicates the presence of a mixture of felsic and mafic minerals (Fig. 1f). A relatively coarse ilmenite grain (80 μm long) is associated with a subrounded plagioclase clast in the upper portion of the Clast E, whereas smaller (20 μm) ilmenites occur in the impact-melt matrix (Fig. 1f).

A lithic clast (Clast F) consisting of an intergrowth between plagioclase and pyroxene is also present in one of our samples (Fig. 2a). The Fe-rich nature of the pyroxene is apparent by its lighter shade in the BSE image compared to nearby relatively Mg-rich clinopyroxene (Fig. 2a). The white-dashed line in the pyroxene grain separates the low-Ca and high-Ca areas, in the upper and lower half, respectively.

EET 96008 contains several clasts comprising large portions of mesostasis areas, typically 200 × 400 μm in size (e.g., Clast G; Fig. 2b). These areas consist of coarse-grained (~20 μm) intergrowths of ferroaugite, fayalite, and interstitial glass. The coarseness of mesostasis minerals indicates slow cooling of the parental magma, normally not associated with lava flows. Such late-stage fractionates of basaltic melts are abundant in the thin sections examined. An example is illustrated in Figure 2c, showing a large crystal of ilmenite (300 μm) surrounded by fayalite. Clast H contains an unusual pyroxene crystal hosting numerous rounded grains of troilite (Fig. 2d).

Apart from the clasts described above, the rest of the meteorite (~80 vol.%) is made up of single-mineral fragments of pyroxene and plagioclase, with minor olivine; the majority of pyroxenes show exsolution lamellae in both plane-polarized light (PPL) and BSE images (Figs. 2e and 2f). Chromite, ulvöspinel, and ilmenite occur throughout the meteorite sample, albeit sparsely, and traces of troilite are present, except in Clast H. This meteorite also contains several globular, silica-rich pods (100–200 μm), some up to 600 μm across. These pods exhibit the typical "crackled" texture, in reflected light, indicative of tridymite.

Some of the textures seen in EET 96008 closely resemble those of EET 87521, Y-793274, and QUE 94281 (EYQ) meteorites, and hence, it is possible that all these meteorites may have come from a similar area of the Moon. We have further compared the mineral chemistry and bulk-rock chemistry of these meteorites to assess the similarity of their source regions. This also addresses possible pairing between EET 87521 and EET 96008, as has been suggested previously by many authors (Mikouchi, 1999; Nishiizumi et al., 1999; Snyder et al., 1999; Warren and Ulff-Møller, 1999).

4. MINERAL CHEMISTRY

Olivine crystals are typically interstitial and much smaller (100–200 μm) than pyroxene crystals (1–2 mm) and display distinctly bimodal compositions ($Fo_{5\text{-}15}$ and $Fo_{60\text{-}65}$). Nevertheless, there is a continuous range in Fo contents from 80 to 0 (Fig. 3c). The fayalitic olivines ($Fo_{5\text{-}15}$) occur almost exclusively in areas showing a late-stage breakdown texture, prob-

Table 1. Representative mineral compositions from various clasts in EET 96008.

	Clast A			Clast B			Clast C			
Wt %	ol	glass	ilm	ferroaugite	plag	usp	ol	opx	plag	plag
SiO_2	30.5	74.7	0.06	46.4	47.2	0.54	37.8	54.4	43.8	46.9
MgO	5.86	0.01	0.50	1.42	0.00	0.09	37.3	26.5	0.10	0.11
CaO	0.34	2.50	0.03	17.9	17.1	0.42	0.29	1.22	19.3	17.6
MnO	0.64	n.a.	0.36	0.47	n.a.	0.38	0.22	0.32	n.a.	n.a.
FeO	62.4	0.51	46.0	31.2	0.55	64.2	24.1	16.5	0.20	0.33
TiO_2	n.a.	n.a.	52.6	1.26	n.a.	32.0	n.a.	0.22	n.a.	n.a.
Al_2O_3	n.a.	14.6	0.01	0.77	32.6	1.26	n.a.	1.26	35.7	33.6
Na_2O	n.a.	3.51	n.a.	0.04	1.54	n.a.	n.a.	<0.03	0.36	1.26
K_2O	n.a.	3.14	n.a.	n.a.	0.09	n.a.	n.a.	n.a.	<0.03	0.08
Cr_2O_3	n.a.	n.a.	0.318	0.02	n.a.	<0.03	n.a.	0.61	n.a.	n.a.
V_2O_3	n.a.	n.a.	n.a.	n.a.	n.a.	0.21	n.a.	n.a.	n.a.	n.a.
ZrO_2	n.a.	n.a.	0.11	n.a.	n.a.	n.a.	n.a.	n.a.	n.a.	n.a.
Total	99.66	98.97	99.98	99.49	99.05	99.06	99.69	100.92	99.50	99.91
Oxygen basis	4	8	3	6	8	4	4	6	8	8
Cations										
Si	0.993	3.254	0.002	1.935	2.191	0.020	0.995	1.956	2.036	2.159
Mg	0.285	0.001	0.019	0.088	0.000	0.005	1.467	1.419	0.007	0.008
Ca	0.012	0.117	0.001	0.800	0.849	0.017	0.008	0.047	0.961	0.866
Mn	0.018	—	0.008	0.016	—	0.012	0.005	0.010	—	—
Fe	1.700	0.019	0.968	1.086	0.021	2.021	0.530	0.495	0.008	0.013
Ti	—		0.994	0.040		0.905	—	0.006		
Al	—	0.747	0.001	0.038	1.783	0.056	—	0.053	1.957	1.824
Na	—	0.296	—	0.003	0.138	—	—	0.000	0.032	0.113
K	—	0.175	—	—	0.005	—	—	—	0.001	0.005
Cr	—	—	0.006	0.001	—	0.000	—	0.017	—	—
V	—	—	0.000	—	—	0.006	—	—	—	—
Total	3.01	4.61	2.00	4.01	4.99	3.04	3.01	4.00	5.00	4.99
Fo/Mg#	14.4	—	—	7.5	—	—	73.5	74.1	—	—
Fs	—	—	—	55.0	—	—	—	25.2	—	—
En	—	—	—	4.5	—	—	—	72.4	—	—
Wo	—	—	—	40.5	—	—	—	2.4	—	—
An	—	—	—	—	85.6	—	—	—	96.7	88.0
Ab	—	—	—	—	13.9	—	—	—	3.2	11.5

	Clast D						Clast E					
Wt %	ol	px	plag	plag	chr	ilm	px	px	px	plag	plag	ilm
SiO_2	38.6	47.5	45.3	44.0	0.13	0.09	52.9	49.6	48.8	50.5	46.2	0.04
MgO	40.3	8.90	0.06	0.03	3.84	0.65	22.0	11.5	11.0	0.03	0.19	0.45
CaO	0.12	8.94	18.2	19.1	0.09	0.06	4.16	8.41	13.4	14.3	17.1	0.15
MnO	0.24	0.45	n.a.	n.a.	0.21	0.40	0.37	0.43	0.32	n.a.	n.a.	0.38
FeO	20.9	30.9	0.44	0.40	35.9	45.3	19.3	27.9	21.7	0.94	1.23	46.3
TiO_2	n.a.	1.08	n.a.	n.a.	9.84	52.2	0.58	0.48	0.78	n.a.	n.a.	51.7
Al_2O_3	n.a.	0.98	33.8	34.9	10.0	0.07	0.92	1.17	2.67	30.3	33.9	0.05
Na_2O	n.a.	0.03	1.03	0.49	n.a.	n.a.	0.03	0.04	0.03	2.70	0.98	n.a.
K_2O	n.a.	n.a.	<0.03	0.05	n.a.	n.a.	n.a.	n.a.	n.a.	0.44	0.12	n.a.
Cr_2O_3	n.a.	0.17	n.a.	n.a.	39.3	0.56	0.24	0.39	0.66	n.a.	n.a.	0.33
V_2O_3	n.a.	n.a.	n.a.	n.a.	0.64	n.a.	n.a.	n.a.	n.a.	n.a.	n.a.	n.a.
ZrO_2	n.a.	n.a.	n.a.	n.a.	n.a.	0.27	n.a.	n.a.	n.a.	n.a.	n.a.	0.17
Total	100.13	98.98	98.85	98.96	99.93	99.64	100.49	99.90	99.31	99.19	99.75	99.54
Oxygen basis	4	6	8	8	4	3	6	6	6	8	8	3
Cations												
Si	0.995	1.931	2.114	2.059	0.004	0.002	1.957	1.953	1.909	2.329	2.136	0.001
Mg	1.550	0.539	0.004	0.002	0.197	0.025	1.211	0.676	0.638	0.002	0.013	0.017
Ca	0.003	0.389	0.912	0.956	0.003	0.002	0.165	0.355	0.561	0.705	0.848	0.004
Mn	0.005	0.015	—	—	0.006	0.009	0.011	0.014	0.010	—	—	0.008
Fe	0.450	1.049	0.017	0.016	1.035	0.956	0.596	0.920	0.709	0.036	0.048	0.981
Ti	—	0.033			0.255	0.989	0.016	0.014	0.023	—	—	0.986
Al	—	0.047	1.862	1.922	0.405	0.003	0.040	0.054	0.123	1.644	1.847	0.002
Na	—	0.003	0.093	0.044	—	—	0.002	0.003	0.002	0.241	0.088	—
K	—	—	0.001	0.003	—	—	—	—	—	0.026	0.007	—

(continued)

Table 1. (Continued)

	Clast D						Clast E					
Wt %	ol	px	plag	plag	chr	ilm	px	px	px	plag	plag	ilm
Cr	—	0.005	—	—	1.070	0.011	0.007	0.012	0.020	—	—	0.007
V	—	—	—	—	0.018	0.002	—	—	—	—	—	0.001
Total	3.00	4.01	5.00	5.00	2.99	2.00	4.01	4.00	4.00	4.98	4.99	2.01
Fo/Mg#	77.5	33.9	—	—	—	—	67.0	42.4	47.4	—	—	—
Fs	—	53.1	—	—	—	—	30.2	47.2	37.2	—	—	—
En	—	27.3	—	—	—	—	61.4	34.6	33.4	—	—	—
Wo	—	19.7	—	—	—	—	8.4	18.2	29.4	—	—	—
An	—	—	90.7	95.3	—	—	—	—	—	72.5	89.9	—
Ab	—	—	9.2	4.4	—	—	—	—	—	24.8	9.3	—

	Clast F			Clast G			Clast H		
Wt %	low-Ca px	high-Ca px	plag	fa	hed	glass	hed		tr
SiO_2	47.4	47.6	45.8	30.5	48.0	98.7	46.7	S	36.2
MgO	6.75	4.98	0.03	5.29	5.56	0.02	0.99	Fe	63.5
CaO	8.95	16.3	18.0	0.27	16.2	0.17	18.3	Co	0.04
MnO	0.48	0.41	n.a.	0.73	0.43	n.a.	0.32	Ni	<0.03
FeO	34.6	27.7	0.62	63.3	27.0	0.93	31.2	Total	99.71
TiO_2	0.72	1.14	n.a.	n.a.	0.81	n.a.	1.12		
Al_2O_3	1.13	1.14	33.7	n.a.	1.35	0.68	1.16	S	49.8
Na_2O	0.04	0.08	1.23	n.a.	0.07	0.09	0.06	Fe	50.1
K2O	n.a.	n.a.	0.07	n.a.	n.a.	0.13	n.a.	Co	0.03
Cr_2O_3	0.24	0.23	n.a.	n.a.	0.11	n.a.	0.07	Ni	—
V_2O_3	n.a.	n.a.	n.a.	n.a.	n.a.	n.a.	n.a.	Total	100
ZrO_2	n.a.	n.a.	n.a.	n.a.	n.a.	n.a.	n.a.		
Total	100.22	99.57	99.38	100.05	99.57	100.73	99.97		
Oxygen basis	6	6	8	4	6	8	8		
Cations									
Si	1.932	1.933	2.127	0.994	1.941	3.953	1.936		
Mg	0.411	0.302	0.002	0.257	0.335	0.001	0.061		
Ca	0.391	0.711	0.894	0.009	0.703	0.007	0.814		
Mn	0.017	0.014	—	0.020	0.015	—	0.011		
Fe	1.179	0.940	0.024	1.725	0.913	0.031	1.082		
Ti	0.022	0.035		—	0.025		0.035		
Al	0.054	0.055	1.845	—	0.064	0.032	0.057		
Na	0.003	0.006	0.111	—	0.006	0.007	0.005		
K	—	—	0.004	—	—	0.007	—		
Cr	0.008	0.007	—	—	0.004	—	0.002		
V	—	—	—	—	—	—	—		
Total	4.02	4.00	5.01	3.01	4.01	4.04	4.00		
Fo/Mg#	25.8	24.3	—	13.0	26.8	—	5.3		
Fs	59.5	48.1	—	—	46.8	—	55.3		
En	20.7	15.5	—	—	17.2	—	3.1		
Wo	19.7	36.4	—	—	36.0	—	41.6		
An	—	—	88.6	—	—	—	—		
Ab	—	—	11.0	—	—	—	—		

Abbreviations: ol-olivine; px-pyroxene; fa-fayalite; opx-orthopyroxene; hed-hedenbergite; plag-plagioclase; ilm-ilmenite; chr-chromite; usp-ulvöspinel; tr-troilite; n.a.-not analyzed.

ably a result of breakdown of Fe-rich metastable pyroxene (Aramovich et al., 2001), except in a few cases such as in Clast A (Fig. 1b; Table 1). Adjacent to Clast B, fine-grained (50–100 μm) fayalite (Fo_{2-3}) is associated with globular tridymite as stringers. The single large (1 mm), euhedral fayalite (Fo_{14-16}) crystal in Clast A contains a central grain of euhedral ilmenite (140 × 200 μm), set at one end of a mass of included glass (Clast A; Fig. 1b). The glass (69.7–74.9 wt.% SiO_2; 1.1–2.6 wt.% K_2O; 14.6–15.2 wt.% Al_2O_3; 3.8–4.0 wt.% Na_2O) also encloses 10- to 40-μm inclusions of whitlockite. This assemblage has all the appearance of the late-stage mesostasis common to most lunar basalts (e.g., Roedder and Weiblen, 1970, 1971, 1972; Taylor et al., 1972; Weiblen and Roedder, 1973).

EET 96008 pyroxene compositions cover almost the entire pyroxene quadrilateral (Figs. 3a and 3b). Single pyroxene fragments range in composition from enstatite ($Wo_{2-3}En_{53-73}Fs_{44-25}$) to pigeonite ($Wo_{16-22}En_{28-58}Fs_{30-54}$) to augite ($Wo_{24-42}En_{22-58}Fs_{24-58}$). Orthopyroxene occurs in Clast C along with fairly Mg-rich olivine (Fo_{73}) and An-rich plagioclase (An_{97}) in an impact-melt matrix (Fig. 1d, Table 1). This clast is classified

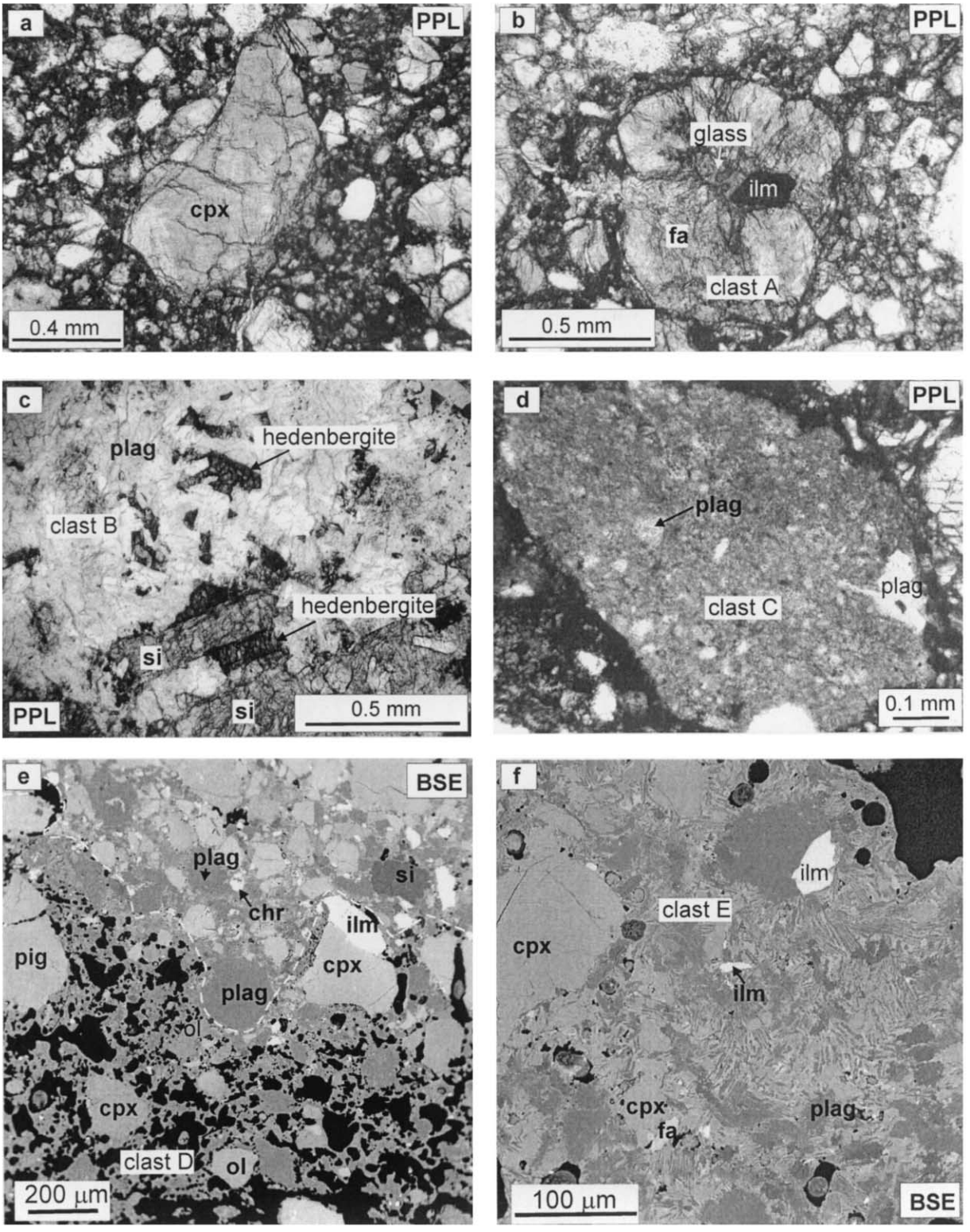

Fig. 1. Photomicrographs and BSE images of different areas and clasts in thin sections of EET 96008. (a) Plane-polarized light (PPL) view of a typical area of the meteorite showing single mineral fragments of pyroxene and plagioclase set is a dark finer-grained matrix. (b) PPL view of "clast A," illustrating the presence of a single ilmenite grain and included glass near the center of a fayalite crystal. (c) PPL view of "clast B" showing the unusual association of hedenbergite with plagioclase and elongated pods of tridymite (si). (d) Transmitted light (TL) view of "clast C" containing grains of opx, ol and plagioclase, making it a norite clast. (e) BSE image of an area showing vesicular texture similar to that seen in many lunar regolith breccias. (f) BSE image of a poorly crystallized impact melt breccia (clast E).

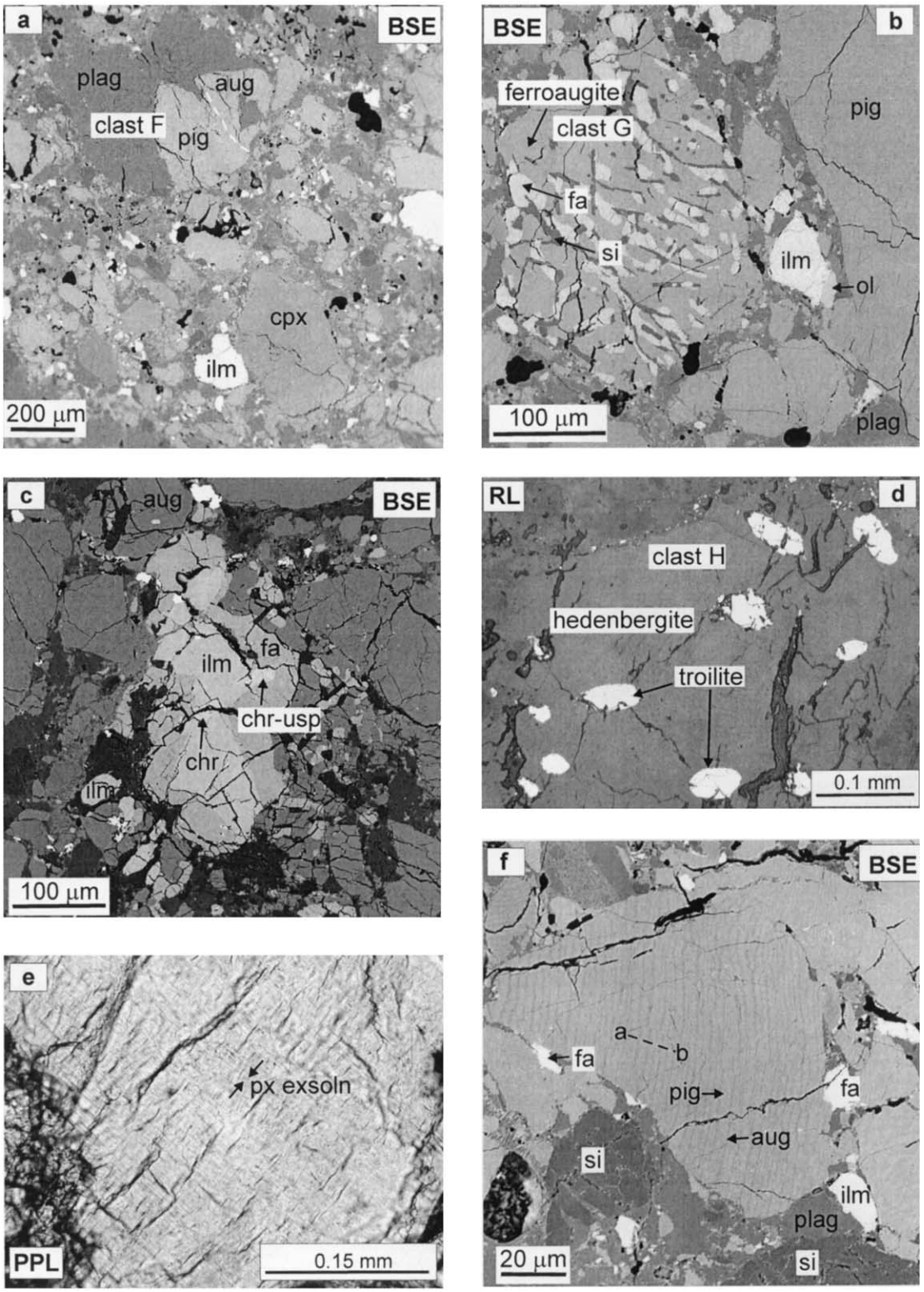

Fig. 2. (a) BSE image showing bi-mineralic clast (clast F) of plagioclase and Fe-rich pyroxene. (b) BSE image showing typical breakdown texture of metastable Fe-rich pyroxene into fayalite (fa), ferroaugite and silica (si). Several such areas exist throughout the thin sections examined. (c) BSE image of a portion of the meteorite consisting of late-stage assemblage, seen in many mare-basalts, consisting of ilmenite, fayalite, ferroaugite, silica and spinels. (d) BSE image of "clast H" consisting of hedenbergite hosting subrounded blebs of troilite. This is one of the most unusual associations seen in a lunar rock. (e) PPL view of a pyroxene grain showing the presence of coarse exsolution lamellaes (by mare standards). (f) BSE image of another pyroxene grain showing the extensive exsolution of augite in pigeonite host.

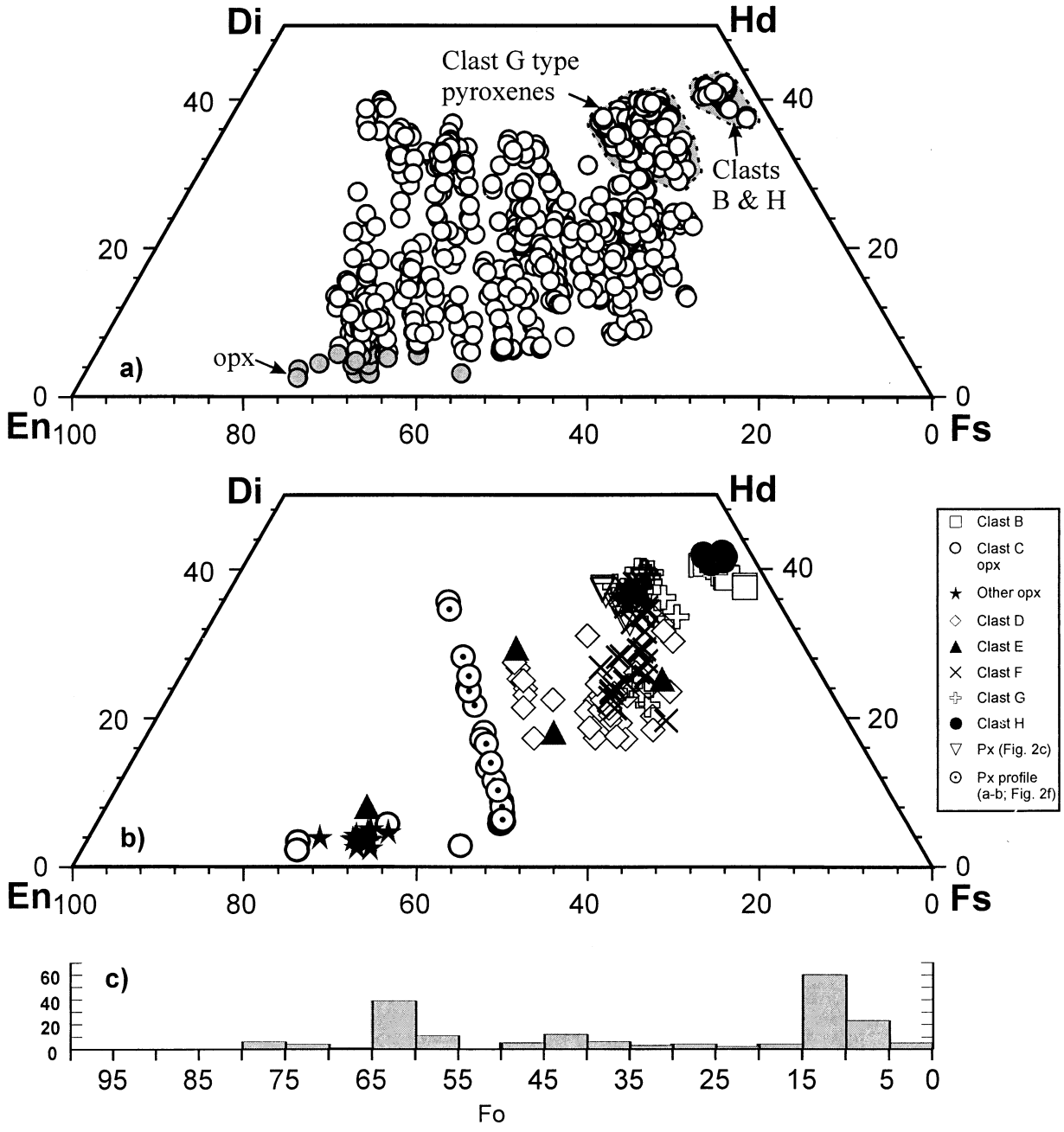

Fig. 3. (a) EET 96008 pyroxene compositions showing wide variations in their mineral chemistry. (b) Pyroxene compositions from individual clast are also plotted to highlight their mineral compositions. Data obtained along a profile through Figure 2f pyroxene are also plotted. (c) Histogram showing the range in Fo contents of olivines from EET 96008.

as "Norite," and its presence shows that EET 96008 has some components that were derived from non-mare source regions. Only two other occurrences of orthopyroxene were seen in the rock, as a single grain and as an intergrowth with olivine. The majority of pyroxene grains are clinopyroxenes and shows extensive exsolution lamellae that are up to 1 μm wide and are easily seen with a petrologic microscope. Augite and pigeonite occur both as host and exsolved phases and vice versa. No inverted pigeonites were found. The presence of exsolution lamellae, as well as their coarseness, resemble those of EET 87521, Y-793274, and QUE 94281 (EYQ) meteorites and suggest slow cooling, in contrast to typical mare-basalts (Mikouchi, 1999). Furthermore, two of these meteorites (EET 87521 and Y-793274) have been reported to contain pyroxene fragments mainly derived from a very-low titanium (VLT) basalt source (Arai et al., 1996).

Several areas or clasts of ferroaugite ($Wo_{35-38}En_{16-18}Fs_{46-47}$), up to 900 μm in longest dimension enclose abundant (up to 30% of the clast), equigranular (20–50 μm) fayalite (Fo_{12-13}) and silica "intergrowths" (Fig. 2b). In some clasts, silica, and to

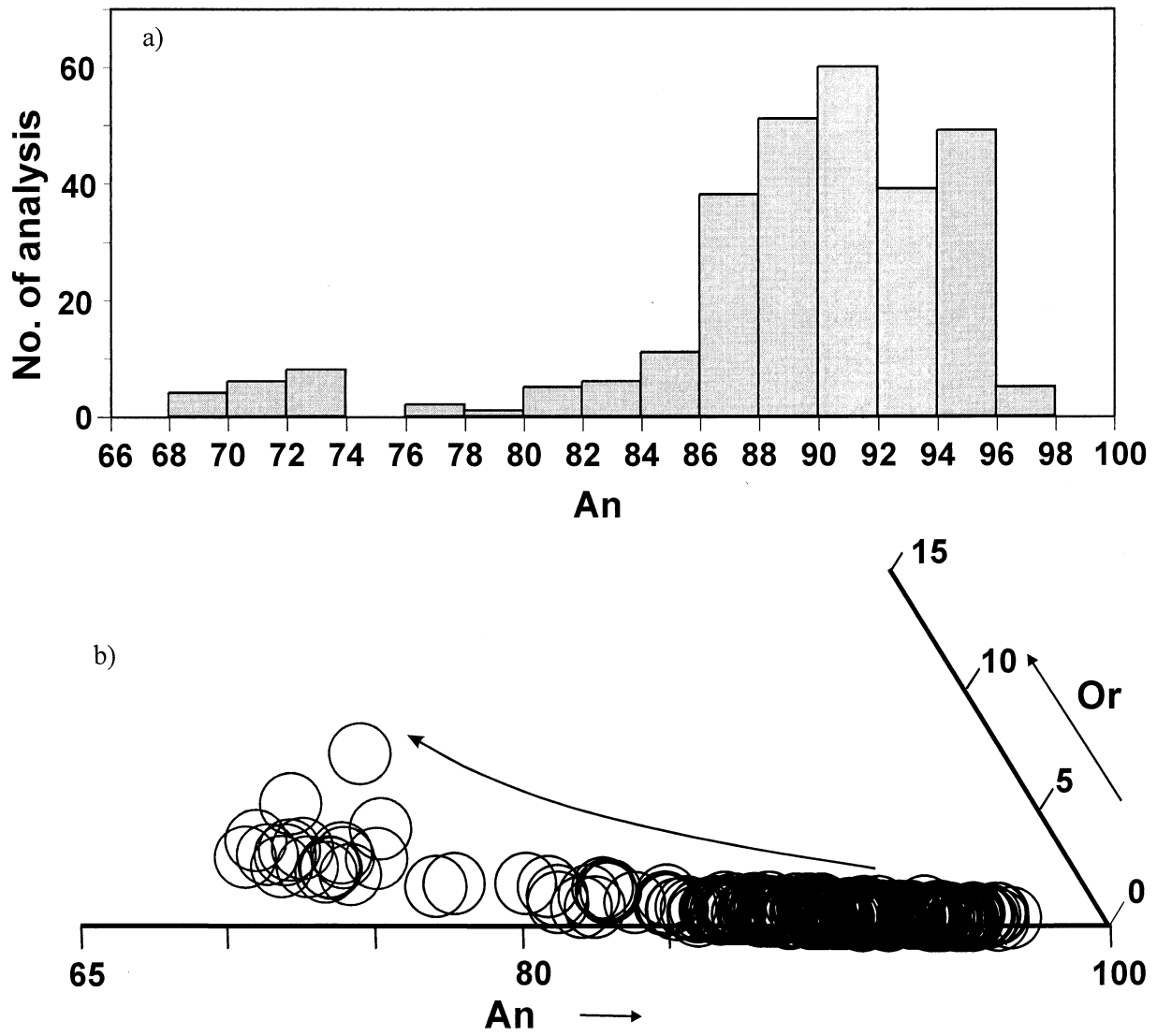

Fig. 4. (a) Histogram showing distribution of An content in EET 96008 plagioclases. (b) Ternary plot for plagioclase compositions shows apparent mare-basalt fractionation trend of increasing Or-content with decreasing An-content.

a lesser extent fayalite, are elongated into stringers or pods, with aspect ratios of 3:1 to 7:1. Such coarse, late-stage mineral assemblages are rare in mare basalts and suggest an unusually slow cooling and strong differentiation of a thick lava flow. This texture probably formed due to the breakdown of metastable Fe-pyroxene, at low pressures, into stable phases such as fayalite, ferroaugite, and silica. However, there is no apparent association of phosphate minerals (whitlockite or apatite) with these breakdown textures. Thus they may represent a simple breakdown of metastable pyroxene, unlike for many Martian meteorites where a two-stage, break-down process has been envisaged by Aramovich et al. (2001).

Clast H, an unusual, nearly pure hedenbergite ($Wo_{42}En_{4\text{-}5}Fs_{53\text{-}54}$) megacryst (600 × 300 μm in size) contains elongated globules (60–70 μm) of troilite (FeS), which may be the result of a breakdown texture that was originally Hd + Fe, with secondary sulfurization of the Fe metal, possibly as a result of impact. In conjunction to this, the total lack of FeNi metal in this sample may reflect an increased oxygen fugacity (albeit still below IW buffer) environment during crystallization of certain components of this breccia; this may also have led to the extreme Fe enrichment seen in the sample.

Plagioclase generally occurs as anhedral masses ($\leq$600 μm) with undulose extinction. Some individual crystals have relict primary textures and twinning, whereas some appear to have been converted to maskelynite. The majority of the plagioclase analyses show a narrow range in An content ($An_{85\text{-}95}$). Plagioclase grains of $An_{95\text{-}97}$ compositions are also present in the sample (Fig. 4a), in minor amount, and occur in clasts that are probably derived from highland-source regions (Clasts C and D; Figs. 1d and 1e; Table 1). An-poor plagioclases ($An_{72\text{-}79}$) generally occur in the vicinity of the mesostasis areas except in one case in which a An-poor plagioclase ($An_{69\text{-}70}$) grain occurs near Clast D. Some of the interstitial, fine-grained, relatively An-poor plagioclase grains ($An_{69\text{-}70}$) are associated with a matrix of K-Si-rich glass (SiO_2 = 71.2–76.1 wt.%; K_2O =

4.6–7.6 wt.%; Al_2O_3 = 11.9–15.6 wt.%; Na_2O = 1.1–3.2 wt.%) and more mafic glasses (SiO_2 = 44.5–48.4 wt.%; Al_2O_3 = 10.9–34.2 wt.%; CaO = 12.4–18.5 wt.%; MgO = 1.8–10.8 wt.%; FeO = 1.5–21.3 wt.%). The ternary plot for plagioclase compositions show an apparent mare-basalt fractionation trend (Fig. 4b).

Clast B consists mostly of subhedral to euhedral, relatively fine-grained (100–300 μm) plagioclase (An_{77-89}; with an aspect ratio of 2:1 to 4:1) and ~5 modal percent hedenbergite ($Wo_{38-42}En_{2-6}Fs_{54-59}$) (Fig. 1c). One end of the clast contains a concentration of tridymite, which comprises ~20% of the total clast, intermingled with small amounts of plagioclase and pyroxene of similar habit to that in the remainder of the clast. Minute (<5 μm) ulvöspinel and ilmenite grains are also present within the clast.

A variety of fine-grained spinel crystals occur throughout the thin section, ranging in composition from ulvöspinel to chromite (Table 1). They show an apparent mare-basalt fractionation trend on Fe# (Fe/[Fe+Mg]) vs. Ti# (Ti/[Ti+Al+Cr]), Fe# vs. Cr# (Cr/[Cr+Al]), and 2Ti-Cr-Al plots (Fig. 5). A single Ti-chromite grain (40.6 wt.% Cr_2O_3; 10.3 wt.% TiO_2; 5.5 wt.% Al_2O_3) from the matrix contains a minute (<5 μm) ilmenite crystal, probably formed by reduction of the ulvöspinel component in the Ti-chromite. This reaction typically occurs at subsolidus temperatures, in a manner similar to that described by Taylor et al. (1972). In one case, a large ilmenite lath (500 μm long) is surrounded by an overgrowth of fayalite. Small grains of chromite and ulvöspinel also occur in this assemblage (Fig. 2c). Crystals of ferroaugite and the breakdown texture of metastable pyroxene are also seen in the vicinity, and in appearance, the assemblage is typical of late-stage mesostasis common to many mare basalts.

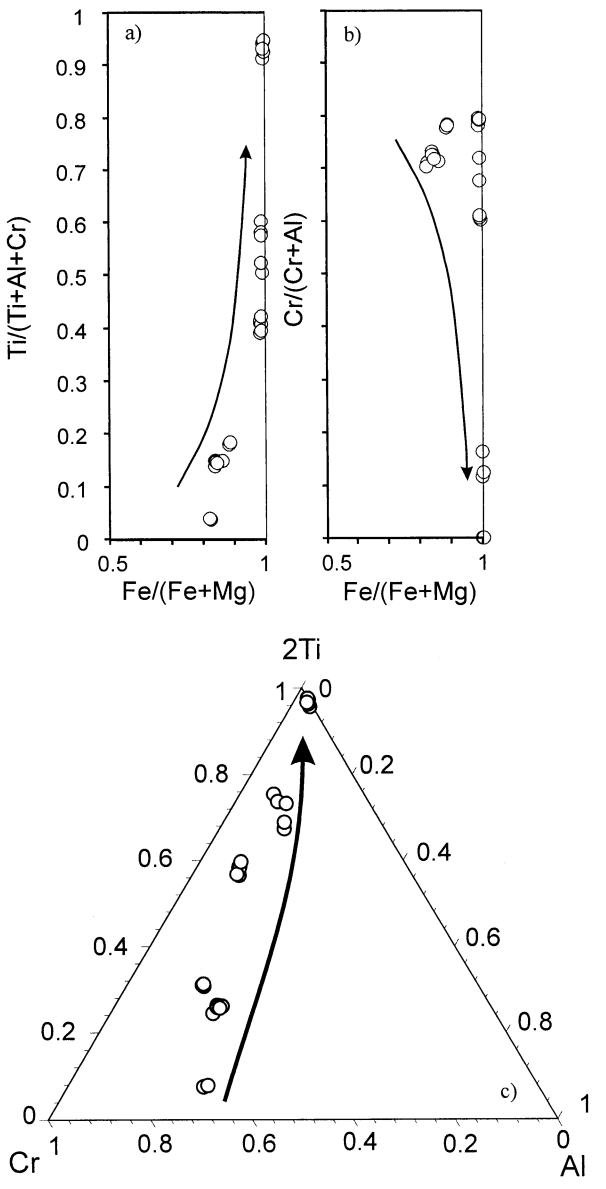

Fig. 5. Plot of Fe# (Fe/[Fe+Mg]) vs. Ti# (Ti/[Ti+Al+Cr]) (a), Fe# vs. Cr# (Cr/[Cr+Al]) (b), and 2Ti-Cr-Al (c) plot for EET 96008 spinels, showing typical mare-basalt fractionation trend.

5. LUNAR ORIGIN AND COMPARISON WITH OTHER LUNAR ROCKS

The following lines of evidence confirm a lunar origin for EET 96008: (1) The atomic Fe/Mn ratios of olivines and pyroxenes in meteorites have been used to discriminate between planetary source regions (Papike, 1998). The Fe/Mn ratios of EET 96008 olivines and pyroxenes follow the lunar trend (Figs. 6a and 6b), thereby providing firm evidence for lunar origin. (2) The age of EET 96008 (3.57 Ga; see section on age dating) is comparable to many low-Ti mare-basalts and is another supporting evidence for the lunar origin for this meteorite. (3) The textural, mineralogical, and geochemical (see section below) similarity of EET 96008 to other lunar meteorites and Apollo mare basalts is also a supportive evidence for lunar origin. (4) The concentrations of cosmogenic radionuclides in EET 96008 are identical to those of EET 87521 and provide strong support for the fact that these two meteorites may be fragments of the same fall. Nishiizumi et al. (1999) postulated that these meteorites were ejected from a depth of 540 to 600 g/cm^2 on the Moon. The transition time from the Moon to the Earth was significantly < 10 ka, and the terrestrial age is 80 ± 30 ka.

Based on the mineralogical studies of two meteorites, EET 87521 and Y-793274, Takeda et al. (1992) concluded that these rocks were derived from a mare region of the Moon. Absence of inverted pigeonite, pyroxene with coarse exsolution lamellaes (>2–3 μm), or orthopyroxenes in granulites suggests minimal contribution from lunar highlands. Similar features are present in our sample (EET 96008), suggesting a close similarity of at least the source regions for these three meteorites. Warren and Ulff-Møller (1999) suggested that based on general compositional-mineralogical similarity between EET 96008/EET 87521 and Y-793274 and QUE 94281, these meteorites are probably launch paired if not paired in the conventional (entry) sense.

As previously noted by some authors (Nielsen and Drake, 1978; Treiman and Drake, 1983), because Ti is incompatible and Cr is compatible in pyroxene structure (Grove and Bence, 1977; Irving, 1978), the Ti# (Ti/[Ti+Cr]) is a useful fractionation indicator. When plotted against Fe#, it characterizes

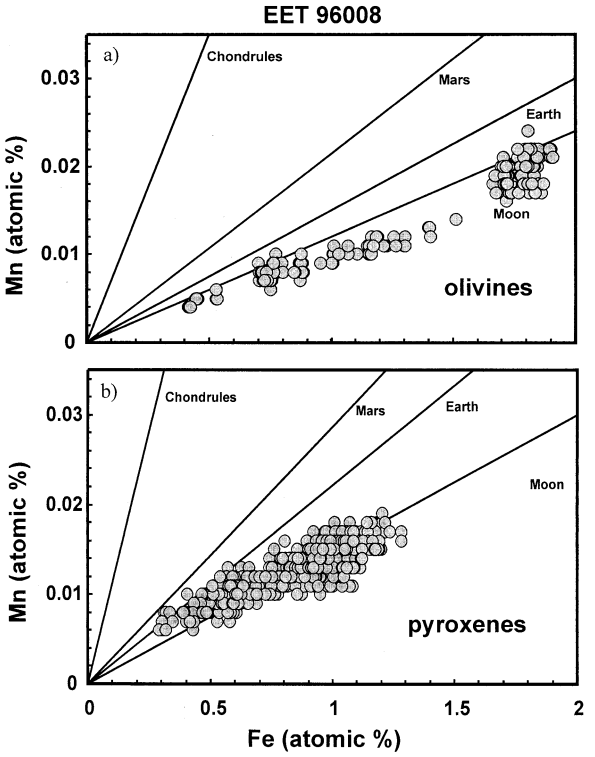

Fig. 6. Plot of Fe/Mn ratio is olivines (a) and pyroxenes (b) from EET 96008. The data follow the lunar trend as evidence for lunar origin.

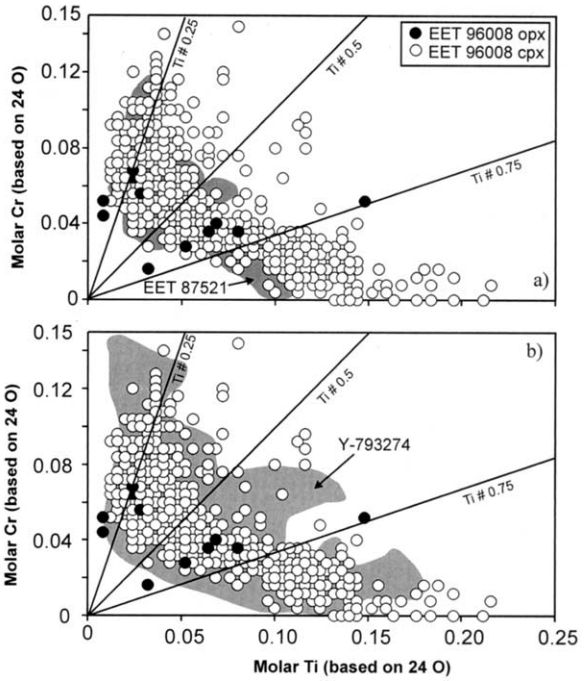

Fig. 7. Ti vs. Cr plot for EET 96008 pyroxenes showing a tight anticorrelation, same as observed in other low-Ti and VLT mare-basalts. Shaded areas in (a) and (b) represent the spread shown by lunar meteorites EET 87521 and Y-793274, respectively (from Arai et al., 1996).

trends depending on the chemical composition of the crystallizing magma. Different pyroxenes in a polymict breccia, such as EET 96008, are not necessarily related, but on the Ti vs. Cr diagram (Fig. 7), they show a relatively tight anticorrelation similar to lunar meteorites, EET 87521 and Y-793274 (shown by shaded regions on Figs. 7a and 7b). Since, these two meteorites have many textural and mineralogical similarities to EET 96008, they have been used frequently for comparison purposes.

On the Fe# vs. Ti# diagram, the pyroxene data from EET 96008 form a pattern comparable to the crystallization trend of pyroxenes from unbrecciated basalts, such as Y-793169 and A-881757, and polymict breccias such as EET 87521, Y-793274, and A-17 VLT basalt suite (Figs. 8a–8c). The orthopyroxene data generally show higher Ti# at relatively lower Fe# compared to rest of the clinopyroxenes in the sample. This is consistent with the orthopyroxene data from regolith breccia Y-793274 and is believed to be a possible highland component. Note the striking similarity between EET 96008 and EET 87521 pyroxenes. The latter meteorite is described as consisting almost entirely of VLT basalt fragments (Warren and Kallemeyn, 1991). This observation provides strong support for the pairing of these two meteorites, while suggesting a possible VLT origin for EET 96008. In addition, the meteorite Y-793274 also shows some similarity to EET 96008 in terms of pyroxene chemistry. However, based on other studies (Takeda et al., 1992; Arai et al., 1996), it would appear that Y-793274 consists mainly of diverse clasts of possible highlands origin, and pyroxenes form a small portion of the meteorite unlike the other two meteorites (EET 96008 and EET 87521), which dominantly consist of mare materials. However, it is still possible that EET 96008 and Y-793274 are paired but without any information on the crystallization ages and cosmic-ray exposure history of the latter, the evidence for pairing is inconclusive.

Nielsen and Drake (1978) and Treiman and Drake (1983) studied Ti# variation in pyroxenes from VLT and low-Ti mare basalts. They suggested that the pyroxene Ti#, at any given Fe#, tends to be systematically lower in VLT basalts than in A-15 low-Ti basalts. However, the comparison must be made at a specific Fe#, because Ti# shows significant dispersion within typically zoned mare pyroxenes, but due to consistent correlation between Fe# and Ti#, the dispersion is small at any given Fe#. The slope of each Fe# vs. Ti# trend is probably sensitive to the variety of additional phases crystallizing together with pyroxene (Arai et al., 1996). However, for rocks with low-Ti (<5 wt.%) contents, the Fe# and Ti# in pyroxene may be directly related to the bulk-rock TiO_2 content. This is because other Ti-rich phases, such as ilmenite, may not have come on the liquidus until late in the crystallization history of the parental magma. Therefore, this relationship between bulk-rock TiO_2 content and pyroxene Ti# (regressed for a Fe# = 0.5 [called $Ti\#_{0.5}$]) can be used effectively to estimate the bulk-rock TiO_2 content of samples that are not entirely composed of mare material or are too small or fragmentary to provide a representative bulk-rock TiO_2 content. We have used a similar approach to that of Arai et al. (1996) to estimate the bulk-rock TiO_2 contents of parental melts from which the majority of the pyroxene grains was derived in a lunar breccia such as EET

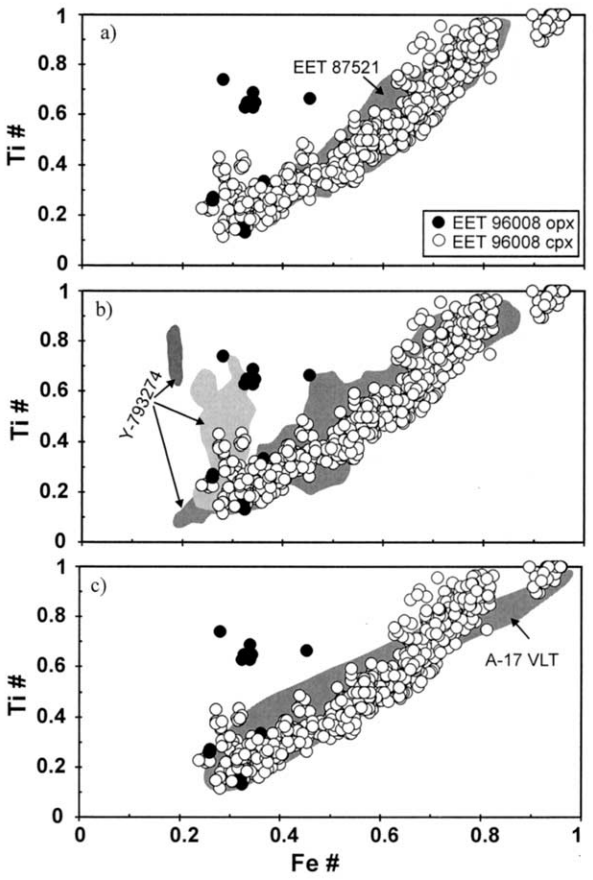

Fig. 8. Plots of Fe# vs. Ti# (Ti/[Ti+Cr]) in EET 96008 pyroxenes. Shaded areas in (a), (b), and (c) are from Arai et al. (1996), representing variation in Fe# and Ti# in EET 87521, Y-793274, and A-17 VLT basalt pyroxenes.

96008. The bulk-rock TiO_2 content determined for polymict breccias by conventional methods can sometimes be ambiguous. It is, therefore, advantageous to be able to constrain the bulk-rock TiO_2 contents by two independent techniques.

Arai et al. (1996) showed that for low-Ti mare basalts, there exists a correlation between their measured bulk-rock TiO_2 content and pyroxene $Ti\#_{0.5}$. A correlation curve, thus obtained, was subsequently used to estimate the bulk-rock TiO_2 content at a given pyroxene $Ti\#_{0.5}$. They also used this approach to estimate bulk-rock TiO_2 contents for some of the low-Ti mare-basalts from A-12 collections and concluded that the estimated TiO_2 content was within $\pm 20\%$ of the measured bulk-rock TiO_2. In the case of EET 96008 pyroxenes, several $Ti\#_{0.5}$ were estimated from different pyroxene trends, and the estimated bulk-rock TiO_2 content is shown as a shaded circle on Figure 9. The size of the circle represents the maximum variation in the regressed $Ti\#_{0.5}$ (0.40–0.47) and estimated TiO_2 content (0.8–1.06), corresponding to the variation on the x- and y-axes, respectively. It is also apparent from Figure 9 that based on this method, EET 96008 pyroxenes can be classified as products of VLT mare-basalt magma, which is consistent with the result of bulk-rock major-element determination, discussed in the next section. The similarity of EET 96008 with EET 87521 and Y793287 meteorites is also highlighted on Figure 9. Also plotted on Figure 9 are the estimated and measured bulk-rock TiO_2 content for the newly discovered, crystalline, low-Ti mare-basalt meteorite, Dh-287A, described by Anand et al. (in press). The estimated and measured values agree well with each other, allowing for reasonable errors associated with regression of pyroxene $Ti\#_{0.5}$, as well as for the possibility of bulk-rock TiO_2 content of Dh-287A being affected by olivine accumulation (Anand et al., in press).

6. MAJOR- AND TRACE-ELEMENT CHEMISTRY

The major-element chemistry of EET 96008 suggests domination by VLT-basaltic components, with TiO_2 contents of 0.75 wt.% and FeO of 18.1 wt.% (Table 2). The overall major-element composition is very similar to EET 87521 and Y-793274 (Table 2). EET 96008 is slightly more aluminous (13 wt.% Al_2O_3) and less calcic (11.2 wt.% CaO) than typical low-Ti mare-basalt. The Al-enriched nature of this meteorite is further highlighted on a plot of Cr vs. Al_2O_3 (Fig. 10). EET 96008 plots, along with EET 87521, towards the lower Cr-, and higher Al_2O_3-end of the mare basalt trend. This plot illustrates two important features of the meteorite. Firstly, it indicates the presence of relatively small amounts of Al-rich highland component in the breccia, consistent with our petrographic observation. Secondly, it clearly shows the relatively evolved nature of the parental magma from which this rock was derived. Only two other mare basalt meteorites (QUE 94281 and Y 793274) have higher Al_2O_3 contents than EET 96008. However, these meteorites are known to contain significant highland-derived components (Arai and Warren, 1999). The other bulk-rock, major-element concentrations of EET 96008 are well within the range for low-Ti mare-basalts. There is, however, substantial variation in trace-elements concentration among the three analyzed whole-rock subsamples of EET 96008 (Table 3). This is probably due to heterogeneous distribution of lithic clasts, as well as the mesostasis, throughout the sample. However, the REE patterns are nearly subparallel, and the average REE concentrations are quite similar to that of EET 87521 (Fig. 11). There is a slight negative Eu anomaly present in REE pattern of the sample, characteristic of low-Ti and VLT mare-basalts. A positive Ce anomaly in one of the subsample (EET 96008, 26) is probably an artifact of terrestrial alteration (Crozaz and Wadhwa, 2001).

For PGE analysis of EET 96008, we combined portions of each subsample that we received to give an average PGE composition for this lunar meteorite (Table 4). It has the highest Ir, Ru, and Pt concentrations analyzed in any low-Ti mare-basalt to date (Fig. 12b). Overall, PGE concentrations in EET 96008 are comparable to EET 87521 and many low-Ti mare basalts (Fig. 12). Warren and Kallemeyn (1991) reported Re, Os, and Ir concentrations from two subsamples of EET 87521: Re = 0.0113 and 0.050 ppb; Os = 0.089 and 0.64 ppb; Ir = 0.095 and 0.51 ppb; Au = 0.059 and 0.22 ppb. The Ir abundance in one of their subsamples is comparable to that reported here (Fig. 12a). However, there is nearly an order of magnitude variation between their two subsamples of EET 87521. This large variation in Ir abundance highlights the heterogeneous nature of EET 87521 as well, similar to that of EET 96008.

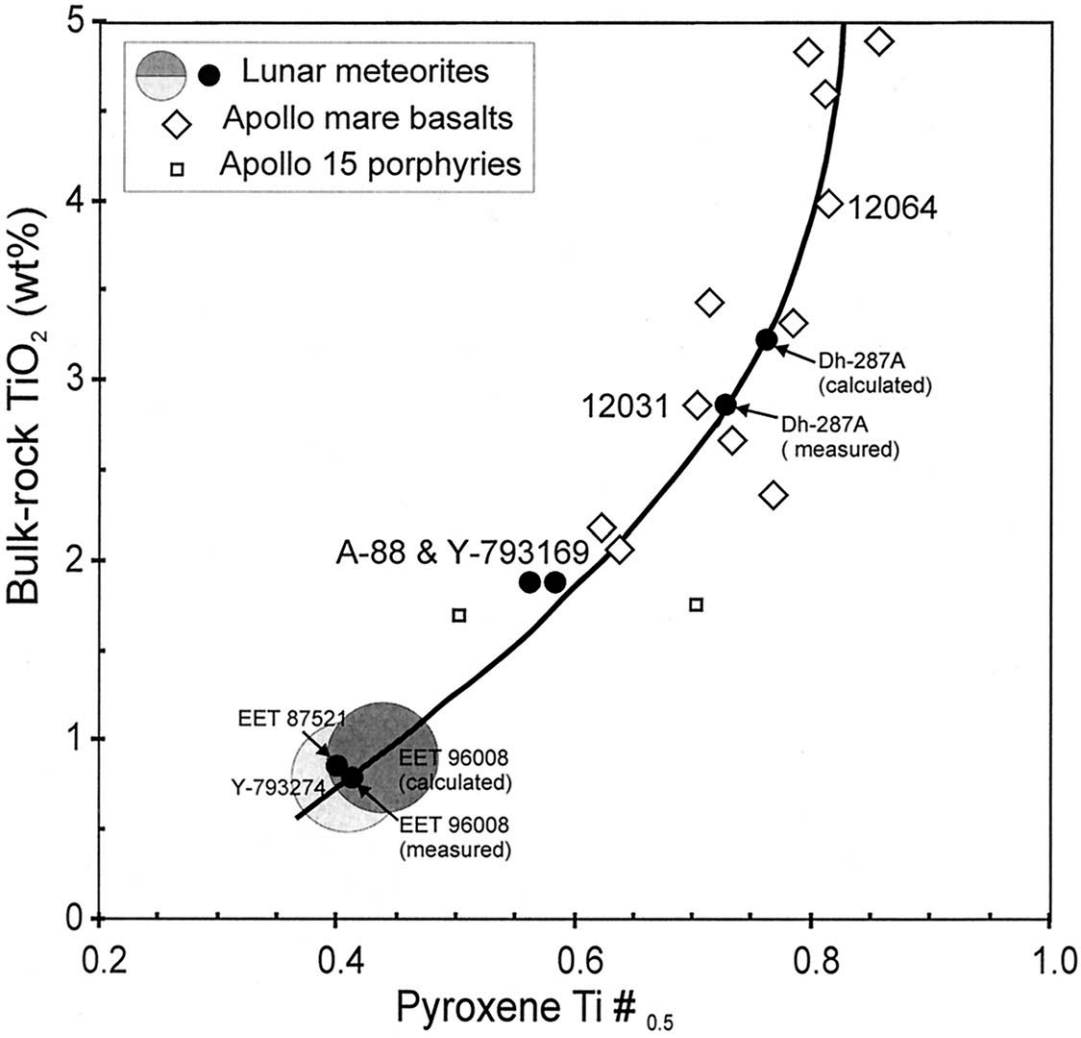

Fig. 9. Plot of Fe#-normalized pyroxene Ti# vs. bulk-rock TiO_2 content for low-Ti and VLT mare basalts. The thick-black curve is the correlation curve obtained using the data for low-Ti crystalline mare-basalt samples for which bulk-rock TiO_2 contents and pyroxene $Ti\#_{0.5}$ are available (modified from Arai et al., 1996). Shaded circles represent spread in pyroxene $Ti\#_{0.5}$ and estimated TiO_2 contents for Y-793274 and EET 96008 meteorites.

6.1. REE of Whitlockite/Apatite

The REE concentrations of apatite and whitlockite (merrillite) in EET 96008 vary over a large range (Table 5). This is highlighted by the abundance of Ce that varies from 1750 ppm in apatite (38.03) to 15,000 ppm Ce in whitlockite (39.04). The sum of the REEs ranges from 5580 to 39,900 ppm. Note that REE concentrations are larger in whitlockite than in apatite, consistent with previous studies of lunar phosphates (e.g., Lindstrom et al., 1985; Neal and Taylor, 1991; Snyder and Taylor, 1992; Jolliff et al., 1993). The chondrite-normalized REE patterns of apatite and whitlockite in the EET 96008 emphasize the large negative Eu anomalies and LREE enrichment typical of lunar phosphates (Fig. 13). However, these are some of the highest REE contents reported for lunar apatite and the lowest for lunar whitlockite (Neal and Taylor, 1991; Jolliff et al., 1993).

6.2. U-Pb Isotopic Compositions and Ages of Phosphates

Radiometric dating of the meteorite can be used to constrain the origin of the components in EET 96008 because mare materials are usually significantly younger than highland rocks (Basaltic Volcanism Study Project, 1981; Taylor, 1982; Snyder et al., 2000). This is the first report of U-Th-Pb dating of phosphates in lunar meteorites. The advantage of this technique over the isotope-dilution thermal-ionization-mass-spectrometry (TIMS) method is the possibility to analyze individual mineral grains, and preservation of textural context, an opportunity for other analytical work to be conducted (such as trace-element measurements), and to collect information on the closure temperature of the U-Pb system (when the cooling rate is available). However, one disadvantage of SHRIMP vs. TIMS method is the large uncertainties associated with the measured ages and hence, a relatively poor temporal resolution among a

Table 2. Major-element composition of EET 96008 from electron microprobe analyses (20) of a fused bead (20 mg). Numbers in parentheses represent the 1 σ variance of the last digit cited.

	EET 96008	EET 87521	A-881757	A-881757	Y-793169	Y-793169	Y-793274	12031	12064
	1	2	3	4	3	4	2,3,5,6,7	8	8
Wt %									
SiO_2	46.5 (2)	47.9	45.4	47.1	43.6	46.1	47.0	47.0	46.3
TiO_2	0.75 (3)	0.97	1.66	2.46	1.52	2.18	0.6	2.88	3.99
Al_2O_3	13.0 (2)	13.2	11.5	10.0	12.9	11.1	16.3	12.6	10.7
Cr_2O_3	0.24 (2)	0.24	0.17	0.29	0.11	0.24	0.27	0.35	0.07
FeO	18.1 (3)	18.8	21.2	22.3	21.2	21.2	14.1	16.8	19.9
MnO	0.24 (2)	0.24	0.25	0.34	0.18	0.32	0.18	0.26	0.27
MgO	7.72 (7)	6.79	6.41	6.25	5.75	5.75	9.25	7.13	6.49
CaO	11.2 (2)	11.6	12.0	11.6	13.3	12.1	12.2	12.3	11.8
Na_2O	0.36 (4)	0.42	0.5	0.25	0.4	0.27	0.41	0.33	0.28
K_2O	0.05 (1)	0.06	0.04	0.04	0.13	0.06	0.08	0.05	0.07
P_2O_5	0.07 (1)	—							
SO_3	0.10* (4)	—							
Total	98.33	100.22	99.05	100.55	98.99	99.26	100.43	99.63	99.86

* Lower limit of SO_3 content in the sample.

Data source: 1, present study; 2, Warren & Kallemeyn (1991); 3, Yanai & Kojima (1991); 4, Warren & Kallemeyn (1993); 5, Koeberl et al. (1991); 6, Fukuoka (1990); 7, Lindstrom et al. (1991); 8, Lofgren & Lofgren (1981).

magmatic suite of samples. The SHRIMP U-Th-Pb dating method using phosphate minerals has been successfully applied to the Shergotty meteorite (Sano et al., 2000). One of the main aims of the present study is to use SHRIMP-derived data from apatite and whitlockite in EET 96008, to place this sample within the chronologic context of its lunar origin.

U, Th, and ^{204}Pb concentrations, $^{238}U/^{206}Pb$, $^{207}Pb/^{206}Pb$, $^{206}Pb/^{204}Pb$, and $^{208}Pb/^{204}Pb$ ratios of apatite and whitlockite in EET 96008 are listed in Table 6. Average Th and U abundances in these phosphates are significantly higher than those in ordinary chondrites (Crozaz et al., 1987) and in Shergotty (Sano et

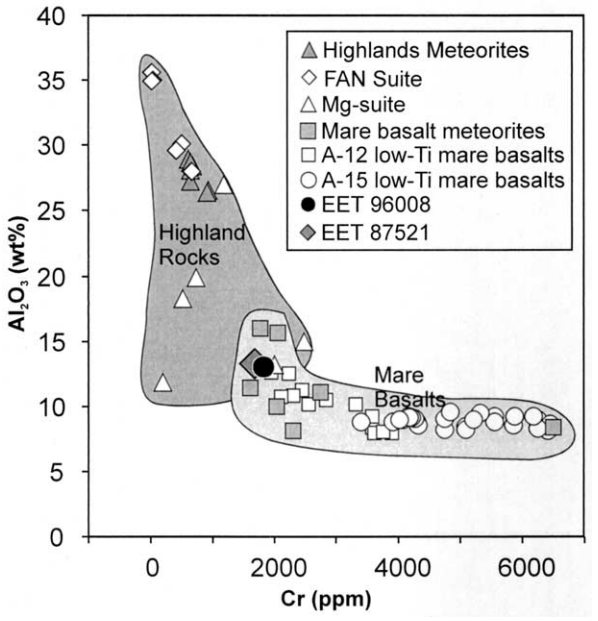

Fig. 10. Plot of Cr vs. Al_2O_3 for lunar rocks. EET 96008 and EET 87521 plot towards the lower Cr- and higher Al_2O_3- end defined by mare basalts. The two envelopes comprise the range shown by lunar mare basalts and highland rocks (meteorites as well as Apollo samples).

Table 3. Trace-Element Abundances (ppm) in three splits of EET 96008 as compared with EET 87521 data by Warren and Kallemeyn (1989).

	EET 96008, 20	EET 96008, 21	EET 96008, 26	EET 87521
Li	4.39	3.99	5.26	—
Be	0.82	0.60	0.99	—
Sc	45.4	40.8	46.7	44
V	103.4	128.2	97	80
Cr	2530	1467	1470	1785
Cu	9.2	8.2	10.7	—
Zn	10.7	5.8	12.6	—
Ga	6.7	6.3	7.4	5.3
Rb	1.4	0.8	1.9	<4
Sr	112.4	109.2	116.8	104
Y	33.4	26.4	39.8	—
Zr	112	94.3	140.8	140
Nb	6.85	5	9.11	—
Mo	0.12	0.09	0.1	—
Cs	0.06	0.02	0.07	0.04
Ba	80.2	48.5	91.7	88
La	7.3	4.69	9.08	8.3
Ce	19.7	12.3	31.4	20.9
Pr	2.84	1.82	3.48	—
Nd	12.7	8.12	15.4	13
Sm	3.65	2.38	4.42	3.86
Eu	0.9	0.7	1	0.98
Gd	4.42	2.88	5.38	—
Tb	0.79	0.52	0.94	0.8
Dy	4.73	3.15	5.73	4.8
Ho	1.05	0.71	1.24	—
Er	2.89	1.87	3.42	—
Tm	0.41	0.28	0.49	—
Yb	2.86	1.92	3.4	3.19
Lu	0.42	0.28	0.5	0.48
Hf	2.42	1.7	3.02	2.88
Ta	0.34	0.22	0.55	0.37
W	0.18	0.09	0.21	—
Pb	0.8	0.24	0.99	—
Th	0.82	0.51	1.1	0.95
U	0.3	0.19	0.35	0.23

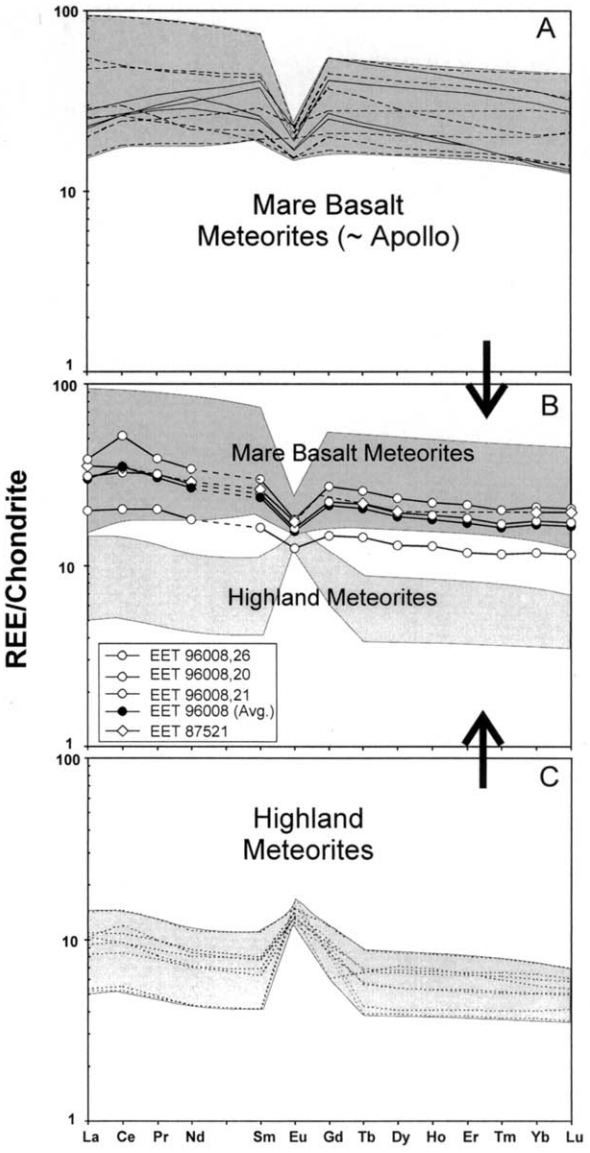

Fig. 11. Chondrite-normalized plot of REE concentrations in three subsamples of EET 96008. The normalization values are from Anders and Grevesse (1989). The average of these three analyses is also plotted and compared with REE patterns from EET 87521, as well as other lunar meteorites. Plots in (A) and (C) illustrate the ranges seen in mare basalt (~Apollo) and highland meteorites. The envelopes from these two plots are only shown with EET data in (B) for clarity.

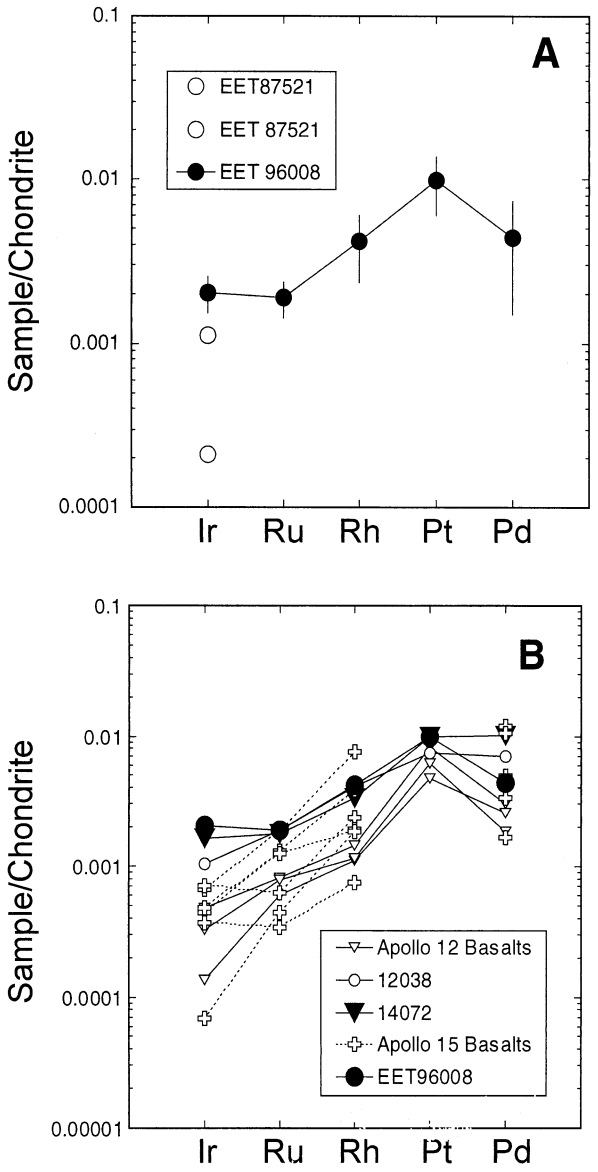

Fig. 12. Chondrite-normalized PGE profile of EET 96008 with 2σ error bars compared to the Ir content of the two EET 87521 aliquots analyzed by Warren and Kallemeyn (1991), and the low-Ti mare basalts. The normalization values are from McDonough and Sun (1995).

Table 4. Platinum-group element abundances in EET 96008 and reproducibility of reference material UMT-1 (Ely et al., 1999). Abundances are in parts per billion (ng/g).

	EET 96008	Error (2 σ)	UMT-1 (Analyzed)	Error (2 σ)	UMT-1 (Certified)	Error (2 σ)
Ru	1.35	0.33	10.40	0.68	10.9	1.5
Rh	0.55	0.24	8.52	0.94	9.5	1.5
Pd	2.43	1.60	103.1	13.6	106	3
Ir	0.93	0.23	8.99	0.99	8.8	0.6
Pt	9.96	3.91	149.1	8.0	129	5

See Ely and Neal (2002) for a description of the method used to calculate the errors associated with the analyses.

Table 5. REE abundances (in ppm) of whitlockite and apatite in EET 96008 that were analyzed by SHRIMP for U-Th-Pb isotopes.

	1	2	3	4	5
La	668	2060	3330	1810	5020
Ce	1750	6730	10,030	5950	15,000
Pr	249	937	1330	994	2020
Nd	1410	4070	5880	4730	8210
Sm	368	1080	1660	1630	2120
Eu	5.52	4504	20	27	66.3
Gd	229	1160	1720	1960	2330
Tb	48.1	204	—	363	372
Dy	391	1030	—	1880	2180
Ho	72.2	186	—	328	410
Er	214	502	—	987	1130
Tm	23.9	65.5	—	133	148
Yb	138	327	—	812	778
Lu	12.7	34.9	78.3	84.4	101
SUM	5580	18,400		21,700	39,900
Eu/Eu*	0.054	0.123	0.036	0.046	0.090
Lu/La	0.019	0.017	0.024	0.047	0.020

Note: Tb to Yb were not analyzed in (3) because of instability of magnetic field. Error of measurement is about 20% estimated by repeated analyses of standard sample, PRAP (Prairie lake apatite, Sano et al., 1999).

Key to samples: 1 = EET 38.03Ap; 2 = EET 39.36Ap; 3 = EET 38.01 Wh; 4 = EET 38.05Wh; 5 = EET 39.04Wh.

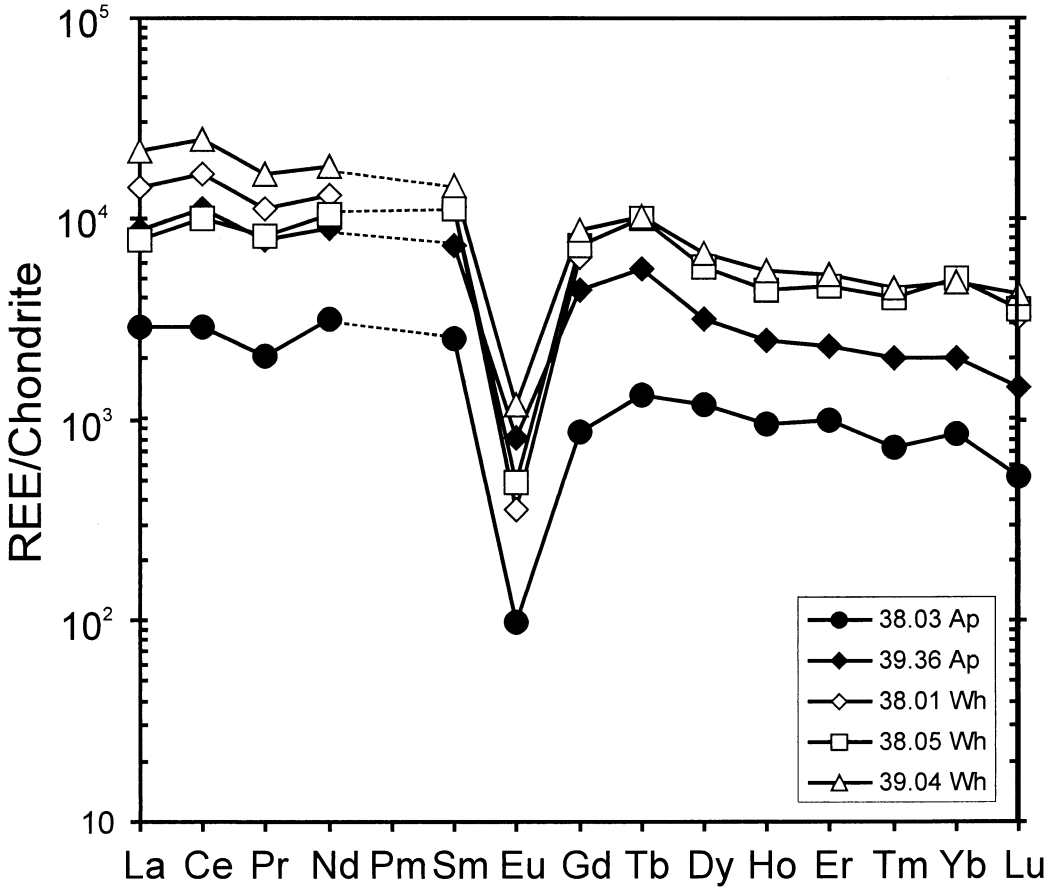

Fig. 13. Chondrite-normalized REE plots of whitlockites and apatites in EET 96008 that were analyzed by SHRIMP for U-Th-Pb isotopes. The normalization values are from Anders and Grevesse (1989).

Table 6. Concentrations of U, Th, and ^{204}Pb, and ratios of ^{238}U/^{206}Pb, ^{206}Pb/^{204}Pb, and ^{208}Pb/^{204}Pb in calcium phosphate in the Lunar Meteorite EET 96008, as measured by SHRIMP II at Hiroshima University, Japan.

Sample	U (ppm)	Th (ppm)	^{204}Pb (ppb)	^{238}U/^{206}Pb	^{207}Pb/^{206}Pb	^{206}Pb/^{204}Pb	^{208}Pb/^{204}Pb
EET38.03Ap	10	15	16	1.22 ± 0.10	0.335 ± 0.015	523 ± 141	210 ± 58
EET39.02Ap	53	88	28	1.41 ± 0.20	0.314 ± 0.021	1329 ± 464	643 ± 227
EET39.06Ap	42	97	24	1.96 ± 0.41	0.331 ± 0.011	902 ± 299	492 ± 166
EET38.05Wh	51	296	17	2.15 ± 0.39	0.325 ± 0.011	1370 ± 1071	926 ± 506
EET38.04Wh	22	193	39	4.53 ± 2.11	0.396 ± 0.026	124 ± 27	220 ± 49
EET39.07Wh	70	196	24	4.52 ± 0.54	0.325 ± 0.017	643 ± 138	400 ± 88
EET38.04Wh	48	343	26	7.78 ± 1.85	0.318 ± 0.015	238 ± 86	419 ± 156
EET38.01Wh	58	265	14	5.78 ± 0.82	0.320 ± 0.013	719 ± 135	830 ± 161

Error assigned to the isotopic and elemental ratio is 1 σ estimated by counting statistics and calibration. Error of concentration is about ±30% estimated by repeated measurements of standard apatite, PRAP (Prairie lake apatite, Sano et al., 1999).

al., 2000). The average Th and U concentrations in apatite are 67 and 35 ppm, and in whitlockite are 259 and 50 ppm, respectively. Both U and Th are highly enriched in these phosphates (Table 6) when compared with the whole-rock abundances (Th = 0.51–1.10 ppm and U = 0.19–0.35 ppm). The average Th/U ratio of 1.9 in apatite is significantly lower than that of 5.2 in whitlockite. There is little difference in ^{204}Pb abundances between apatite and whitlockite, varying only from 14 to 39 ppb, respectively.

The positive correlation between ^{204}Pb/^{206}Pb and ^{207}Pb/^{206}Pb ratios (Fig. 14) can be explained by either a true radiogenic ^{206}Pb*-^{207}Pb* isochron age or the mixing between two components, such as in situ radiogenic Pb and common Pb. If the correlation has age significance, it represents a ^{206}Pb*-^{207}Pb* isochron age of 3530 ± 270 Ma (2σ; MSWD = 0.25; rec = 0) for apatite and 3519 ± 100 Ma (2σ; MSWD = 0.97; rec = 0) for whitlockite. The positive correlation in the ^{204}Pb/^{206}Pb-^{207}Pb/^{206}Pb diagram could also be attributed to the mixing of two components. If so, three-dimensional linear regressions for the total Pb/U isochron in a ^{238}U/^{206}Pb-^{207}Pb/^{206}Pb-^{204}Pb/^{206}Pb diagram would also result in a valid age estimate (Wendt, 1989). This was the case for the Shergotty phosphates, where a concordia constrained a linear 3-D isochron age of 217 ± 110 Ma (Sano et al., 2000). In contrast, due to the complex history of EET 96008 such a 3-D linear regression is not suitable to the EET 96008 phosphates. In such scenarios where a secondary event might have affected the U-Pb systematics, 3-D planar regression is preferred. Thus, we have calculated a 3-D planar regression of the whitlockite and apatite data in ^{238}U/^{206}Pb-^{207}Pb/^{206}Pb-^{204}Pb/^{206}Pb space using Isoplot/Ex v. 2.49 program (Ludwig, 2001). Distribution of the phosphate data in the 3-D diagram intercepts a plane where ^{204}Pb/^{206}Pb = 0, which in turn defines the discordia that is defined by the dotted line in Figure 15. This discordia yields a lower concordia-intercept age of 100 ± 130 Ma (2σ), taken as zero, and an upper intercept of 3569 ± 100 Ma (2σ), within error of the ^{206}Pb*-^{207}Pb* ages.

7. DISCUSSION

Warren and Ulff-Møller (1999) reported petrographic similarities between EET 87521 and EET 96008, such as coarse-pyroxene exsolution, decomposed coarse-pyroxferroite clasts, and an extremely evolved, Fe-rich clast (96e). This led to their conclusion that like EET 87521, EET 96008 is comprised of nearly pure VLT-mare material. However, Mikouchi (1999) noted two features of EET 96008 that were thought to be inconsistent with an extrusive mare-basalt origin. Firstly, the exsolution lamellae in the pyroxenes are too coarse by mare-standards. Secondly, Ti-rich and Fe-poor pyroxenes were reported as being probably of a highlands affinity. Nevertheless, similar coarse (0.2–1 μm) exsolution features were seen in many other lunar meteorites (e.g., Y-793274 and EET 87521), containing dominantly pyroxene component from VLT source (Takeda et al., 1992; Arai et al., 1996). Certainly, all authors agree that it is a unique situation for mare basalts and perhaps, a common but not universal feature of VLT-basalt flow. The Ti-rich and Fe-poor pyroxenes most probably are of highlands affinity, but they are present is such minor amount in EYQ meteorites that they do not warrant much attention beside the possibility that there are some non-mare components in these samples.

Fe-rich metastable pyroxene clasts of the size and associations described here are unusually coarse-grained and have not been observed in mare basalts; when occurring in mare basalts, Fe-rich metastable pyroxene often occur as rims surrounding evolved pyroxene grains and as small grains in mesostasis (e.g., Roedder and Weiblen, 1970; Weiblen and Roedder, 1973). The evolved mineralogies of EET 96008 indicate that the apparent VLT component is atypical for returned mare-basalt samples of this composition. Rather, the magma from which the majority of EET 96008 components were derived had experienced a high degree of fractional crystallization, as evidenced by the over-abundance of ferroaugite. Other petrographic features of EET 96008 (and EET 87521) are also consistent with extreme fractional crystallization of a mare-basalt melt. For example, the abundance of tridymite, high K-Si glass, and fayalite-augite-tridymite pods. Finally, the presence of a large fayalite crystal (Clast A) that contains ilmenite engulfed by K-Si-rich glass and whitlockite is consistent with a melt undergoing a high degree of fractional crystallization to the point where the residual liquid undergoes silicate liquid immiscibility (SLI, e.g., Neal and Taylor, 1989). The liquid had split into a K-rich and REE + P-rich fractions (the "K-frac." and "REEP-frac." of Neal and Taylor, 1988, 1989, 1991). An example of such extreme fractional crystallization in a mare basalt was reported by Lu et al. (1989), who found the assemblage fayalite + silica

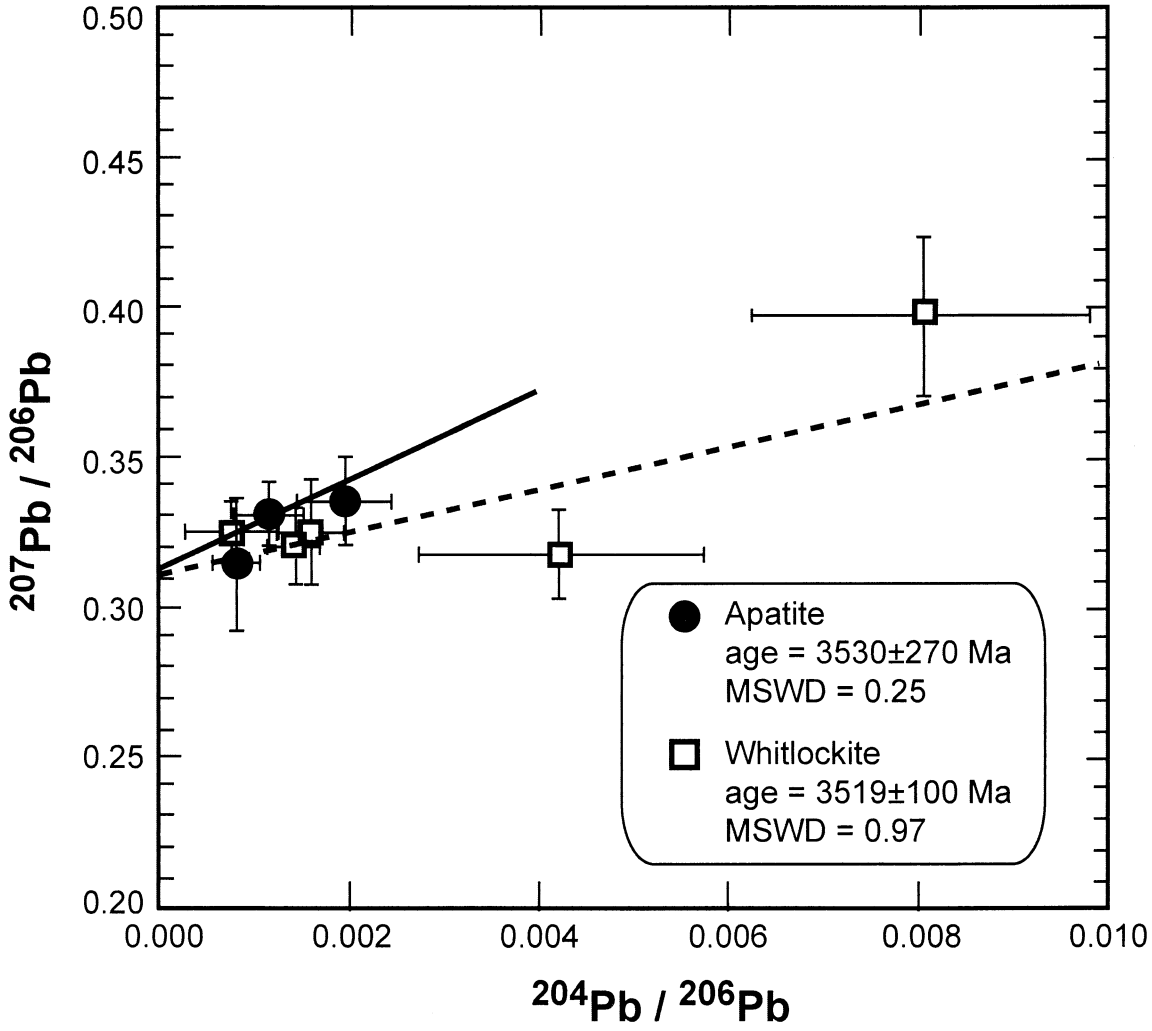

Fig. 14. Correlation of $^{204}Pb/^{206}Pb$ and $^{207}Pb/^{206}Pb$ ratios of apatite and whitlockite in the lunar meteorite EET 96008. Errors are portrayed at the 1σ level. Lines show the best fit by the York method (York, 1969).

+ phosphate in a LUNA 24 basalt. This assemblage was interpreted as a good representation of the "REEP-fraction" after SLI.

Pyroxene fragments in EET 96008 show a fractionation trend remarkably similar to those of A-17 VLT basalts. In addition, the Fe# vs. Ti# plots for EET 96008 pyroxenes show similar trends defined by pyroxenes from lunar meteorites EET 87521 and Y-793274, providing evidence for similar basaltic precursors for these meteorites. The estimated bulk-rock TiO_2 content of EET 96008, based on pyroxene Fe#-normalized Ti# trends, is very similar to the measured concentration and further indicates that there is minimal contamination from non-mare materials.

The trace element data of EET 96008 are comparable to many low-Ti mare basalts, and the Cr vs. Al_2O_3 plot highlights its highly fractionated nature and the presence of some highland-derived components. In terms of V and (to a lesser extent) Cr, both EET 96008 and EET 87521 have relatively low concentrations compared to low-Ti mare basalts, further confirming their relatively evolved nature. However, it should be re-iterated that there is indication that this rock has been affected by terrestrial weathering (e.g., elevated LREEs, in particular a positive Ce anomaly in one of the subsample), in spite of general lack of observable petrographic evidence. Nevertheless, there is a large variation in the bulk-rock REE contents from three subsamples that has been interpreted to be due to the heterogeneous nature of this rock.

As shown on the Cr vs. Al_2O_3 plot (Fig. 10), comparison with other mare basalts and highland meteorites shows that EET 96008 plots towards the lower Cr boundary and upper Al region of the pattern defined by mare basalts, but close to the upper Cr end and lower Al region of the trend defined by highland rocks. This feature is another supporting piece of evidence for the significantly evolved nature of EET 96008 parental magma in comparison to other mare basalt magmas, and a possibility of limited mixing with highland-derived components. The PGE data also suggest a mare precursor for EET 96008 constituent minerals. In comparison with pristine mare basalts, EET 96008 falls in the upper range defined by the low-Ti basalts (Fig. 12). The Ir abundance in EET 96008 plots

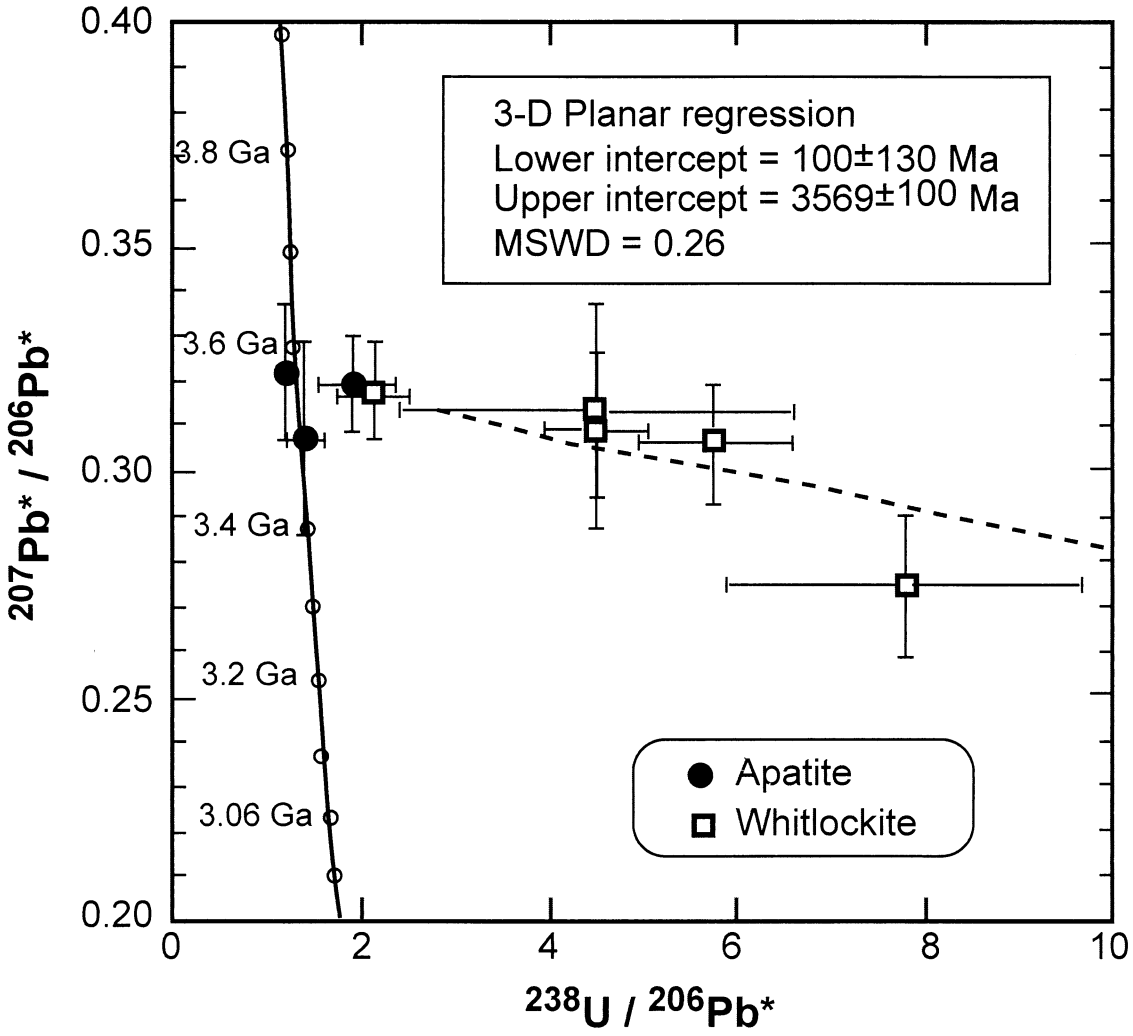

Fig. 15. A result of three-dimensional planar regressions of apatite and whitlockite in the lunar meteorite EET 96008 for the total Pb/U isochron. All data are projected onto the $^{238}U/^{206}Pb^*$- $^{207}Pb^*/^{206}Pb^*$ plane. Errors are portrayed at the 1σ level. The dotted line shows the best fit by the Isoplot/Ex v. 2.49 (Ludwig, 2001).

slightly above the low-Ti basalt field (Fig. 12), possibly indicating incorporation of a small extraterrestrial component.

7.1. Ages of Phosphates and Lunar Chronology

The 3569 ± 100 Ma U-Pb discordia age documents the primary formation of the phosphates, probably related to magmatic activity. Note that whitlockite is more influenced by a shock event than apatite since its ^{238}U-$^{206}Pb^*$ age is significantly younger than that of the apatite; an observation that is quite different to earlier studies of Shergotty (Sano et al., 2000). This may be partly due to differences in grain sizes of the apatite and whitlockite.

The chronology of lunar rocks based predominantly on Apollo samples, has been well documented (see review by Snyder et al., 2000). The Rb-Sr and Sm-Nd crystallization ages of are basalts range from 3.1 to 3.9 Ga, with a few as old as 4.3 Ga. The observed formation age of 3569 ± 100 Ma for the EET 96008 phosphates is significantly younger than that of all highland rocks. These ages are within errors of the low-Ti basalts dated from the Apollo 12 and 15 sites (Snyder et al., 2000). Therefore, it is considered likely that the EET 96008 phosphates are derived from lunar mare materials.

The cosmic-ray exposure history of EET 87521, based on the noble gas contents and the ^{26}Al, ^{10}Be, ^{36}Cl and ^{41}Ca activities, as reported by Vogt et al. (1993), showed that this lunar sample was launched from the Moon $< 10^5$ yr ago and arrived on the Earth between 15 and 50×10^3 yr ago. Nishiizumi et al. (1999) suggested that the exposure history of EET 96008 is compatible with that of EET 87521. The lower-intercept "age" of 100 ± 130 Ma recorded in the EET 96008 phosphates, although with a huge error, is at least consistent with both launch and arrival time. It is possible that the discordia found in the ^{238}U-$^{206}Pb^*$ age of the phosphates in EET 96008 are attributable to shock metamorphism. In addition to the exposure history, Vogt et al. (1993) reported a K-Ar age of EET 87521 in the range 3.0 to 3.4 Ga, which is slightly younger than the EET 96008 phos-

phate formation of 3569 ± 100 Ma. The age discrepancy may be due to radiogenic ^{40}Ar loss related to the shock event as revealed in the discordia of U-Pb system. Thus, it is still considered likely that the ages are the same, at least for the mare-basalt components in EET 87521 and EET 96008.

8. SUMMARY

Lunar meteorite EET 96008 is dominantly composed of material derived from a VLT basalt magma that experienced extreme fractional crystallization to the point of silicate-liquid immiscibility. The nature of the mare component is indicated by the textural, mineralogical and geochemical similarities with many of the known low-Ti and VLT basalts. The coarse exsolution features in pyroxenes, coarse grain sizes of metastable Fe-rich pyroxene, hedenbergite, tridymite, fayalite, ferroan augite, and K-rich glass are consistent with very slow and extreme fractional crystallization of a magma either ponded in a lava lake or in an unusually thick VLT basalt flow.

U-Pb and Pb-Pb ages derived from whitlockite and apatite in EET 96008 are younger than highlands rocks and are interpreted to represent the age of the basaltic component. The ages are within error of the Apollo 12 and Apollo 15 low-Ti mare basalts. The PGE contents of EET 96008 fall within the range defined by low-Ti mare basalts, except for Ir, which is slightly elevated, possibly indicating the presence of a small extraterrestrial component.

The petrography, mineral chemistry, and major- and trace-element chemistry of EET 96008 are nearly indistinguishable from those of lunar meteorite EET 87521. Therefore, we concur with previous suggestions that these two lunar meteorites are paired and should, therefore, share the same petrogenetic history.

Acknowledgments—Jinesh Jain and James C. Ely are thanked for their help in conducting trace-element and PGE analyses, respectively, at Notre Dame University. Dawn Taylor is thanked for helping with the figures. Hayami Ishisako and Yasuhiro Shibata aided with sample preparation at Hiroshima. The manuscript has benefited greatly from constructive reviews and criticism by Christine Floss and an anonymous reviewer. This is a joint contribution from the Planetary Geosciences Institute at Tennessee and the SHRIMP Laboratory at Hiroshima. A portion of this study was supported by NASA Grant NAG 5-8154 and NAG 59158 (to LAT) and NAG 5-8099 (to CRN), for which we are grateful.

Associate editor: C. Koeberl

REFERENCES

Anand M., Misra K. C., Taylor L. A., Nazarov M., and Demidova S. I. (in press) Lunar meteorite Dhofar 287A: A new lunar mare basalt. *Meteorit. Planet. Sci*.

Anders E. and Grevesse N. (1989) Abundances of the elements: Meteoritic and solar. *Geochim. Cosmochim. Acta* **53,** 197–214.

Arai T. and Warren P. H. (1999) Lunar meteorite Queen Alexandra Range 94281: Glass compositions and other evidence for launch pairing with Yamato 793274. *Meteorit. Planet. Sci.* **34,** 209–234.

Arai T., Takeda H., and Warren P. H. (1996) Four lunar mare meteorites: Crystallization trends of pyroxenes and spinels. *Meteorit. Planet. Sci.* **31,** 877–892.

Aramovich C. J., Herd C. D. K., and Papike J. J. (2001) Possible causes for late-stage reaction textures associated with pyroxferroite and metastable pyroxenes in the basaltic Martian meteorites [abstract]. *Lunar Planet. Sci.* **32,** abstract no. 1003, CD-ROM.

Basaltic Volcanism Study Project. (1981) Lunar Mare basalts. In *Basaltic Volcanism on the Terrestrial Planets*, pp. 236–281. Pergamon, New York.

Crozaz G. and Wadhwa M. (2001) The terrestrial alteration of Saharan Shergottites Dar al Gani 476 and 489: A case study of weathering in a hot desert environment. *Geochim. Cosmochim. Acta* **65,** 971–978.

Crozaz G., de Chazal S., Lundberg L. L., Zinner E., Pellas P., and Bourt-Denise M. (1987) Actinides and rare earth elements in chondrites. *Meteoritics* **22,** 362–363.

Ely J. C. and Neal C. R. (2002) Method of data reduction and uncertainty estimation for platinum-group element data using inductively coupled plasma-mass spectrometry. *Geostandards Newsletter* **26,** 31–39.

Ely J. C., Neal C. R., O'Neill J. A., and Jain J. C. (1999) Quantifying the platinum group elements (PGEs) and gold in geological samples using cation exchange pretreatment and ultrasonic nebulization inductively coupled plasma-mass spectrometry (USN-ICP-MS). *Chem. Geol.* **157,** 219–234.

Fukuoka T. (1990) Chemistry of Yamato-793274 lunar meteorite. In *NIPR Symp. Antarct. Meteorites XV*, pp. 122–123. Tokyo, Japan.

Grove T. L., and Bence A. E. (1977) Experimental study of pyroxene-liquid interaction in quartz-normative basalt 15597. In *Proc. Lunar Sci. VIII*, pp. 1549–1579. Pergamon, New York.

Irving A. J. (1978) A review of experimental studies of crystal/liquid trace element partitioning. *Geochim. Cosmochim. Acta* **42,** 743–770.

Jolliff B. L., Haskin L. A., Colson R. O., and Wadhwa M. (1993) Partitioning in REE-saturating minerals: Theory, experiment, and modelling of whitlockite, apatite, and evolution of lunar residual magmas. *Geochim. Cosmochim. Acta* **57,** 4069–4094.

Koeberl C., Kurat G., and Brandstatter F. (1991) Lunar meteorite Yamato-793274: Mixture of mare and highland components, and barringerite from the Moon. In *NIPR Symp. Antarct. Meteorites IV*, pp. 33–55. Tokyo, Japan.

Lindstrom M. M., Crozaz G., and Zinner E. (1985) REE in phosphates from lunar highland cumulates: An ion microprobe study [abstract]. *Lunar Planet. Sci.* **16,** 493–494.

Lindstrom M. M., Mittlefehlt D. W., Martinez R., Lipschutz M. E., and Wang, M. S. (1991) Geochemistry of Yamato-82191, -86032, and -793274 lunar meteorites. In *NIPR Symp. Antarct. Meteorites IV*, pp. 12–32. Tokyo, Japan.

Lofgren G. E. and Lofgren E. M. (1981) *Catalog of Lunar Mare Basalts Greater Than 40 Grams.* Lunar and Planetary Contribution 438. NASA Johnson Space Center, Houston, Texas.

Lu F., Taylor L. A., and Jin Y. (1989) Basalts and gabbros from Mare Crisium: Evidence for extreme fractional crystallization. In *Proc. Lunar Planet. Sci. XIX*, pp. 199–208. Pergamon, New York.

Ludwig K. R. (2001) *Users Manual for Isoplot/Ex v. 2.49: A Geochronological Toolkit for Microsoft Excel*. Berkeley Geochronology Center Special Publication No. 1a.

McDonough W. F. and Sun S. (1995) The composition of the Earth. *Chem. Geol.* **120,** 223–253.

Mikouchi T. (1999) Mineralogy and petrology of a new lunar meteorite EET 96008: Lunar basaltic breccia similar to Y-793274, QUE 94281 and EET 87521 [abstract]. *Lunar Planet. Sci.* **30,** abstract no. 1558, CD-ROM.

Neal C. R. (2001) Interior of the Moon: The presence of garnet in the primitive deep lunar mantle. *J. Geophys. Res. Planet.* **106,** 27865–27885.

Neal C. R. and Taylor L. A. (1988) "K-Frac + REEP-Frac": A new understanding of KREEP in terms of granite and phosphate petrogenesis [abstract]. *Lunar Planet. Sci.* **19,** 831–832. CD-ROM.

Neal C. R. and Taylor L. A. (1989) Metasomatic products of the lunar magma ocean: The role of KREEP dissemination. *Geochim. Cosmochim. Acta* **53,** 529–541.

Neal C. R. and Taylor L. A. (1991) Evidence for metasomatism of the lunar highlands and the origin of whitlockite. *Geochim. Cosmochim. Acta* **55,** 2965–2980.

Nielsen R. J. and Drake M. J. (1978) The case for at least three mare basalt magmas at the Luna 24 landing site. In *Mare Crisium: The View From Luna 24* (eds. R. B. Merrill and J. J. Papike), pp. 419–428. Pergamon, New York.

Nishiizumi K., Masarik J., Caffee M. W., Jull A. J. T. (1999) Exposure histories of paired lunar meteorites EET 96008 and EET 87521 [abstract]. *Lunar Planet. Sci.* **30,** abstract no. 1980, CD-ROM.

Papike J. J. (1998) Comparative planetary mineralogy: Chemistry of melt-derived pyroxene, feldspar, and olivine. In *Planetary Materials, Vol. 36* (ed. J. J. Papike), pp. 7.1–7.11. Mineralogical Society of America, Washington, DC.

Roedder E. and Weiblen P. W. (1970) Lunar petrology of silicate melt inclusions, Apollo 11 rocks. In *Proc. Apollo 11 Lunar Sci.*, pp. 801–837. Pergamon, New York.

Roedder E, and Weiblen P. W. (1971) Petrology of melt inclusions, Apollo 11 and Apollo 12 and terrestrial equivalents. In *Proc. Lunar Sci. II*, pp. 507–528. Pergamon, New York.

Roedder E, and Weiblen P. W. (1972) Petrographic features and petrologic significance of melt inclusions in Apollo 14 and 15 rocks. *Proc. Lunar Sci. III*, pp. 251–279. Pergamon, New York.

Sano Y., Oyama T., Terada K., and Hidaka H. (1999) Ion microprobe U-Pb dating of apatite. *Chem. Geol.* **153,** 249–258.

Sano Y., Terada K., Takeno S., Taylor L. A., and McSween H. Y. Jr. (2000) Ion microprobe uranium-thorium dating of Shergotty phosphates. *Meteorit. Planet. Sci.* **35,** 341–346.

Snyder G. A., and Taylor L. A. (1992) Petrogenesis of the western highlands of the Moon: Evidence from a diverse group of whitlockite-rich rocks from the Fra Mauro Formation. *Proc. Lunar Planet. Sci. XXII*, pp. 399–416. Pergamon, New York.

Snyder G. A., Neal C. R., Taylor L. A., and Halliday A. N. (1997) Anatexis of lunar cumulate mantle in time and space: Clues from trace-element, strontium, and neodymium isotopic chemistry of parental Apollo 12 basalts. *Geochim. Cosmochim. Acta* **61,** 2731–2747.

Snyder G. A., Neal C. R., Ruzicka A. M., and Taylor L. A. (1999) Lunar meteorite EET 96008, part II. Whole-rock trace-element and PGE chemistry, and pairing with EET87521 [abstract]. *Lunar Planet. Sci.* 30, abstract no. 1705.

Snyder G. A., Borg L. E., Nyquist L. E., and Taylor L. A. (2000) Chronology and isotopic constraints on lunar evolution. In *Origin of the Earth and Moon* (eds. R. M. Canup and K. Righter), pp. 361–396. The University of Arizona Press, Tucson.

Takeda H., Mori H., Saito J., and Miyamoto M. (1992) Mineralogical studies of lunar mare meteorites EET 87521 and Y 793274 [abstract]. In *Proc. Lunar Planet. Sci. XXII*, pp. 355–364. Pergamon, New York.

Taylor L. A., Kullerud G., and Bryan W. B. (1972) Opaque mineralogy and textural features of Apollo 12 samples and a comparison with Apollo 11 rocks. In *Proc. Lunar Sci. II*, pp. 855–871. Pergamon, New York.

Taylor S. R. (1982) *Planetary Science: A Lunar Perspective*. Lunar & Planetary Institute, Houston, TX.

Treiman A. H. and Drake M. J. (1983) Origins of lunar meteorite ALHA81005: Clues from the presence of terrae clasts and a very low titanium basalts clast. *Geophys. Res. Lett.* **10,** 783–786.

Vogt S., Herzog G. F., Eugster O., Michel T., Niedermann S., Krähenbuhli U., Middleton R., Dezfouly-Arjomandy B., Fink D., and Klein J. (1993) Exposure history of the lunar meteorite, Elephant Moraine 87521. *Geochim. Cosmochim. Acta* **57,** 3793–3799.

Warren P. and Ulff-Møller F. (1999) Lunar meteorite EET96008: Paired with EET 87521, but rich in diverse clasts [abstract]. *Lunar Planet. Sci.* **30,** abstract no. 1450.

Warren P. H. and Kallemeyn G. W. (1989) Elephant Moraine 87521: The first lunar meteorite composed of predominantly mare material. *Geochim. Cosmochim. Acta* **53,** 3323–3330.

Warren P. H. and Kallemeyn G. W. (1991) Geochemical investigation of five lunar meteorites: Implications for the composition, origin and evolution of the lunar crust. In *NIPR Symp. Antarct. Meteorites IV*, pp. 91–117. Tokyo, Japan.

Warren P. H. and Kallemeyn G. W. (1993) Geochemical investigation of two lunar mare meteorites: Yamato-793169 and Asuka-881757. In *NIPR Symp. Antarct. Meteorites VI*, pp. 35–37. Tokyo, Japan.

Weiblen P. W. and Roedder E. (1973) Petrology of melt inclusions in Apollo samples 15598 and 62295, and of clasts in 67915 and several lunar soils. In *Proc. Lunar Sci. IV*, pp. 681–703. Pergamon, New York.

Wendt I. (1989) Geometric considerations of the three-dimensional U/Pb data presentation. *Earth Planet. Sci. Lett.* **94,** 231–235.

Yanai K. and Kojima H. (1991) Varieties of lunar meteorites recovered from Antarctica. In *NIPR Symp. Antarct. Meteorites IV*, pp. 70–90. Tokyo, Japan.

York D. (1969) Least squares fitting of a straight line with correlated errors. *Earth Planet. Sci. Lett.* **5,** 320–324.